© 2021. Published by The Company of Biologists Ltd | Development (2021) 148, dev199772. doi:10.1242/dev.199772

RESEARCH ARTICLE

# An epigenetic circuit controls neurogenic programs during neocortex development

**Andi Wang[1,*], Junbao Wang[1,*], Kuan Tian[1], Dawei Huo[2], Hanzhe Ye[1], Si Li[3], Chen Zhao[1], Bo Zhang[1], Yue Zheng[1], Lichao Xu[1], Xiaojiao Hua[1], Kun Wang[1], Qing-Feng Wu[4], Xudong Wu[3], Tao Zeng[2,‡], Ying Liu[1,‡] and Yan Zhou[1,‡]**

## ABSTRACT

The production and expansion of intermediate progenitors (IPs) are essential for neocortical neurogenesis during development and over evolution. Here, we have characterized an epigenetic circuit that precisely controls neurogenic programs, particularly properties of IPs, during neocortical development. The circuit comprises a long non-coding RNA (*LncBAR*) and the BAF (SWI/SNF) chromatin-remodeling complex, which transcriptionally maintains the expression of *Zbtb20*. *LncBAR* knockout neocortex contains more deep-layer but fewer upper-layer projection neurons. Intriguingly, loss of *LncBAR* promotes IP production, but paradoxically prolongs the duration of the cell cycle of IPs during mid-later neocortical neurogenesis. Moreover, in *LncBAR* knockout mice, depletion of the neural progenitor pool at embryonic stage results in fewer adult neural progenitor cells in the subventricular zone of lateral ventricles, leading to a failure in adult neurogenesis to replenish the olfactory bulb. *LncBAR* binds to BRG1, the core enzymatic component of the BAF chromatin-remodeling complex. *LncBAR* depletion enhances association of BRG1 with the genomic locus of, and suppresses the expression of, *Zbtb20*, a transcription factor gene known to regulate both embryonic and adult neurogenesis. ZBTB20 overexpression in *LncBAR*-knockout neural precursors reverses compromised cell cycle progressions of IPs.

**KEY WORDS: Neocortex, Intermediate progenitor cells, BAF complex, Long non-coding RNA, ZBTB20**

## INTRODUCTION

The mammalian neocortex of the cerebrum, which is the structure underlying cognition and intellectual ability, is a six-layered structure largely composed of excitatory/projection neurons (PNs) (Caviness and Rakic, 1978). Neocortical PNs are exclusive derivatives of radial glial progenitors (RGs). RGs are neural progenitor cells (NPCs) encompassing apical RGs (aRGs) and basal RGs (bRGs), with bRGs being more abundant in gyrencephalic brains (Florio and Huttner, 2014). Throughout cortical neurogenesis, RGs give rise to intermediate (basal) progenitors (IPs), which translocate to the subventricular zone (SVZ), then become committed neuronal progenitors that may divide for a few rounds before generating PNs. The emergence and expansion of cortical IPs, also known as transit amplifying, are believed to be essential for neocortex formation and enlargement during development and evolution (Haubensak et al., 2004; Kriegstein et al., 2006; Molyneaux et al., 2007; Noctor et al., 2004). IPs directly produce most, if not all, PNs of different neocortical layers (Kowalczyk et al., 2009). Intriguingly, unlike RGs, neocortical IPs are committed neuronal progenitors and lack retrograde plasticity (Mihalas et al., 2016; Oberst et al., 2019; Qian et al., 2000). Thus, it is of great interest to unveil cellular and molecular machineries governing fate choices of neocortical IPs.

Although neurogenesis mostly occurs prenatally, adult neurogenesis persists in two areas of the mammalian brain: the ventricular-subventricular zone (V-SVZ) in the walls of the lateral brain ventricles; and the subgranular zone (SGZ) of the dentate gyrus of the hippocampus (Kriegstein and Alvarez-Buylla, 2009). Adult neural stem cells (aNSCs) at V-SVZ produce neuronal progenies that migrate along the rostral migratory stream (RMS) to replenish interneurons in the olfactory bulb (OB) (Zhao et al., 2008). Recent studies have shown that aNSCs at V-SVZ are derived from a slowly dividing subpopulation of embryonic neural progenitors (Fuentealba et al., 2015; Furutachi et al., 2015). Therefore, the abundance and cellular status of embryonic NPCs would have impacts on aNSC lineages.

Proper cell cycle control is essential for maintaining NPC pools and producing neural progenies (Arai et al., 2011; Calegari et al., 2005), and is largely the intrinsic property that sets the appropriate timing of neurogenesis (Dubreuil et al., 2000; Dyer and Cepko, 2001; Geng et al., 2018). Manipulating cell cycle progress of NPCs, including that of IPs, could change the neurogenic program. For example, overexpression of Cdk4/cyclin D1 enhances the generation and expansion of IPs, leading to a thicker subventricular zone and larger surface area of the neocortex (Lange et al., 2009). On the other hand, slowing the cell cycle of embryonic NPCs using the CDK inhibitor p57 is probably essential for establishing the adult NSC pool (Furutachi et al., 2015). However, little is known about how cell cycle control of NPCs, particularly IPs, is precisely regulated and coordinated with neurogenesis in neocortex development.

Recent progresses have uncovered crucial roles for epigenetic mechanisms – chromatin structures at multiple dimensions, nucleosome components and arrangements, histone modifications,

[1]Frontier Science Center for Immunology and Metabolism, Medical Research Institute at School of Medicine, Department of Neurosurgery, Zhongnan Hospital of Wuhan University, College of Life Sciences, Wuhan University, Wuhan, China 430071. [2]Department of Neurosurgery, Shanghai Tenth People's Hospital, Tongji University School of Medicine, Shanghai, China 200072. [3]State Key Laboratory of Experimental Hematology, The Province and Ministry Co-Sponsored Collaborative Innovation Center for Medical Epigenetics, Tianjin Key Laboratory of Cellular Homeostasis and Human Diseases, Department of Cell Biology, School of Basic Medical Sciences, Tianjin Medical University, Tianjin, China 300070. [4]State Key Laboratory of Molecular Development Biology, Institute of Genetics and Developmental Biology, Chinese Academy of Sciences, Beijing, China 100101.
*These authors contributed equally to this work

‡Authors for correspondence (ztbox73@163.com; y.liu@whu.edu.cn; yan.zhou@whu.edu.cn)

K.W., 0000-0001-5910-1568; Q.-F.W., 0000-0003-3272-6247; Y.Z., 0000-0002-2713-4442

**Handling Editor: Paola Arlotta**
**Received 1 May 2021; Accepted 8 October 2021**

Development (2021) 148, dev199772. doi:10.1242/dev.199772

modifications of DNA, RNA and long non-coding RNAs – in controlling cellular behaviors and fate choices during neocortex development (Chalei et al., 2014; Ramos et al., 2015; Wang et al., 2017; Yao et al., 2016; Yoon et al., 2018). The SWI/SNF complex, also known as the BRG1- or BRM-associated factors (BAF) complex, is a subfamily of ATP-dependent chromatin remodeling complexes that provides essential nucleosome rearrangement, allowing genes to be activated or repressed (Narayanan and Tuoc, 2014; Sokpor et al., 2017). Components of the BAF complex have been found to be crucial in neocortical development, with variable roles in controlling the IP pool (Narayanan et al., 2018, 2015; Nguyen et al., 2016; Tuoc et al., 2013). However, it remains to be elucidated how the activity of the BAF complex is conveyed into the control of specific gene expressions, and hence cell proliferation and differentiation during neocortical development.

Here, we unveil a previously unidentified epigenetic circuit encompassing the BAF chromatin-remodeling complex, a long non-coding RNA (*LncBAR*) and the transcription factor ZBTB20, which tightly controls transit amplification of IPs during cortical neurogenesis. Loss of *LncBAR* enhances the association of the BAF complex with the genomic region of *Zbtb20*, thus repressing its expression, which hampers division of IPs and reduces generation of upper-layer IPs. Re-expressing ZBTB20 reverted compromised IP divisions in *LncBAR* knockout neocortices.

## RESULTS

### Disproportionate neocortical layering in *LncBAR*-null brains

We have previously screened lncRNAs with spatiotemporal expression specificities in developing mouse neocortex, followed by characterizing lncRNAs with *cis*-regulatory roles in controlling transcription of adjacent/overlapping protein-coding genes (PCGs) (Li et al., 2020; Tian et al., 2021). Here, we identified an intergenic lncRNA gene (*LncBAR* – BAF-associated lncRNA) that contains a single exon and is expressed in developing mouse forebrains. The *LncBAR* gene is associated with H3K36me3, a histone modification indicative of active gene transcription, in developing forebrains, with its transcripts predominantly residing in nuclei (Fig. S1A-C). *In situ* hybridization detected the expression of *LncBAR* transcripts throughout the dorsal and ventral forebrain (Fig. S1C,D). In adult tissues, *LncBAR* is relatively abundant in the brain (Fig. S1E). The transcript of *LncBAR* is 2.85 kb long, which was validated by 5′ and 3′ rapid amplification of cDNA ends (Fig. S1F), and northern blotting (Fig. S1G), with its protein-coding scores aligned with those of lncRNAs that include *Hotair*, *Malat1* and *Paupar* but not PCGs (Fig. S1H). Notably, sequence comparison showed that transcripts with high sequence homology to *LncBAR* could not be identified in primates.

To explore the function of *LncBAR* in brain development, we generated *LncBAR* knockout (KO) mice using CRISPR/Cas9-mediated gene editing. Homozygous *LncBAR*$^{KO}$ mice were born at mendelian ratio without gross abnormalities; they thrive and are fertile (Fig. S2A-D). Intriguingly, the neocortex area and thickness of adult *LncBAR*$^{KO}$ brains were slightly reduced, with a thinner layer II-IV but a thicker layer V-VI compared with wild-type controls. These data were not statistically significant (Fig. S2E-I) but prompted us to examine whether loss of *LncBAR* has any effects on neocortical layer structures. Immunofluorescent (IF) staining and quantification analyses showed *LncBAR*$^{KO}$ neocortices had more CTIP2$^{+}$ and FOXP2$^{+}$ (not statistically significant) deep-layer projection neurons (PNs) and significantly fewer SATB2$^{+}$ and CUX1$^{+}$ upper-layer PNs (Fig. 1A-E). Next, 5-bromo-2′-deoxyuridine (BrdU, a synthetic thymidine analogue) was injected at embryonic day (E) 13.5 or E15.5 to label newborn cells at respective time points, and neocortex sections were examined at postnatal day (P) 7 (Fig. 1F,I). At P7, many deep-layer (CTIP2$^{+}$) or upper-layer (SATB2$^{+}$) PNs were labeled with BrdU and were properly localized in control brains. In *LncBAR*$^{KO}$ neocortices, more PNs were labeled at E13.5 with a larger proportion of BrdU$^{+}$ cells residing in superficial regions (Fig. 1G, H), whereas significantly fewer PNs were labeled at E15.5 with a larger proportion of BrdU$^{+}$ cells localizing in deeper regions (Fig. 1J,K). Together, *LncBAR* is essential for neurogenic program of the developing neocortex.

### Loss of *LncBAR* leads to overproduction of IPs but stalls their cell cycle progression

We next turned to dorsal forebrains at E16.5, when deep-layer PNs have been produced and upper-layer PNs are being born (Greig et al., 2013). Consistent with findings in the adult stage, neocortex length and area were reduced in E16.5 *LncBAR*$^{KO}$ brains (Fig. S3A-C). More specifically, CTIP2$^{+}$ deep-layer PNs were slightly overproduced but SATB2$^{+}$ upper-layer PNs were significantly fewer in the *LncBAR*$^{KO}$ neocortex, emphasizing the altered neurogenic programs during embryonic neocortex development (Fig. 2A-C and Fig. S3D). Cleaved caspase 3 staining excluded enhanced apoptosis in *LncBAR*$^{KO}$ neocortices (Fig. S3F,G).

We next investigated expression of markers for RGs (PAX6$^{+}$) and IPs (TBR2$^{+}$) to examine the progenitor pool. Although numbers of PAX6$^{+}$ RGs were not altered in E16.5 *LncBAR*$^{KO}$ neocortices (Fig. 2D,E and Fig. S3E), numbers of TBR2$^{+}$ IPs were significantly increased, with more PAX6$^{+}$TBR2$^{+}$ co-expressing cells (Fig. 2D,F,G and Fig. S3E). This indicates enhanced production and/or hampered differentiation of IPs upon loss of *LncBAR* (Fig. 2H). Overproduction of TBR2$^{+}$ IPs and increased PAX6$^{+}$TBR2$^{+}$ co-expression were also prominent in E13.5 *LncBAR*$^{KO}$ dorsal forebrains (Fig. 2I-M). Notably, numbers of PAX6$^{+}$ RGs were slightly lower in E13.5 *LncBAR*$^{KO}$ dorsal forebrains (Fig. 2J). Therefore, loss of *LncBAR* causes overproduction of IPs, more deep-layer PNs but, paradoxically, fewer upper-layer PNs.

We next examined whether the cell cycle progression of IPs was altered in *LncBAR*$^{KO}$ neocortices. BrdU was injected to label S-phase cells at E15.5 and embryos were collected at E16.5 for immunofluorescence analyses (Fig. S4A). Although equal amounts of cortical cells incorporated BrdU during the 24 h period, a smaller proportion of BrdU$^{+}$ cells co-expressed Ki67 (a marker indicative of actively cycling cells) in *LncBAR*$^{KO}$ neocortices, suggesting more cells have exited from the active cell cycle (Fig. S4B-D). We then looked into the cell cycle progression of IPs. Triple labeling with BrdU (24 h), Ki67 and TBR2 showed that significantly fewer TBR2$^{+}$ IPs were cycling in *LncBAR*$^{KO}$ neocortices: a larger proportion of *LncBAR*$^{KO}$ TBR2$^{+}$ IPs incorporated BrdU during the 24 h period but fewer IPs were Ki67 positive (Fig. 3A-D). Moreover, there were fewer TBR2$^{+}$BrdU$^{+}$Ki67$^{+}$ cells and a smaller proportion of TBR2$^{+}$BrdU$^{+}$ IPs expressing Ki67 in *LncBAR*$^{KO}$ neocortices (Fig. 3E,F). Most importantly, cell-cycle measurements using sequential EdU and BrdU labeling showed *LncBAR*$^{KO}$ IPs had longer overall cell-cycle time, as well as a longer S-phase period (Fig. 3G-K). Intriguingly, at E13.5 – the time when deep-layer PNs are produced (Greig et al., 2013) – significantly more Ki67$^{+}$TBR2$^{+}$ double-labeled cells were present in *LncBAR*$^{KO}$ neocortices, suggesting more *LncBAR*$^{KO}$ IPs were in active cell cycle (Fig. S4E-M). Together, in *LncBAR*$^{KO}$ neocortices, overproduced IPs generate more deep-layer PNs at earlier stages, but the defect of IP divisions at mid-later neurogenesis causes compromised production of upper-layer PNs.

Development (2021) 148, dev199772. doi:10.1242/dev.199772

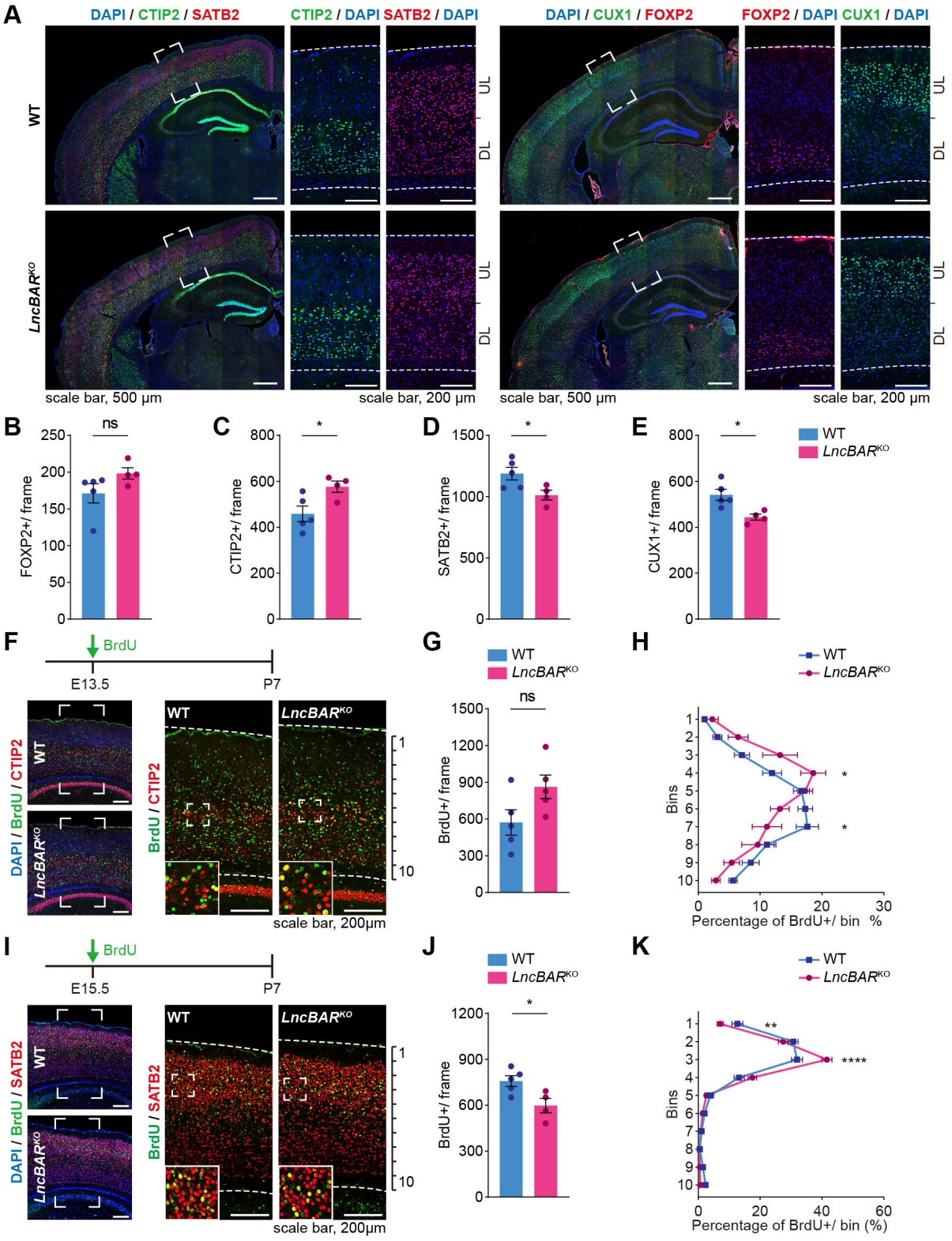


**Fig. 1.** See next page for legend.

### *LncBAR* depletion diminishes the pool of adult neural stem cells at the V-SVZ

Notably, the olfactory bulbs (OBs) of adult *LncBAR*$^{KO}$ brains were significantly smaller than control brains (Fig. 4A-E), indicating compromised adult neurogenesis and/or defects of neuroblast migration/differentiation upon loss of *LncBAR*. Interneurons of OBs, including those expressing TBR2, calretinin (CR) and calbindin (CB), are continuously replenished by migrating doublecortin-expressing neuroblasts that are generated by aNSCs in the V-SVZ of the walls of the lateral brain ventricles. Detailed analyses showed that the glomerular layer (GLL) and granule cell layer (GCL) areas were smaller (Fig. S5A-D) and numbers of TBR2$^{+}$, CR$^{+}$ but not CB$^{+}$

Development (2021) 148, dev199772. doi:10.1242/dev.199772

**Fig. 1. Ablation of *LncBAR* altered neocortical neurogenesis.** (A) Double immunofluorescence images of CTIP2/SATB2 (left) and FOXP2/CUX1 (right) staining on adult wild-type and *LncBAR*$^{KO}$ neocortices. Nuclei were labeled with DAPI (blue). Outlined regions are enlarged on the right. (B-E) Quantification of FOXP2 (B), CTIP2 (C), SATB2 (D) and CUX1 (E) positive neurons in A. *n*=5 for wild-type brains and *n*=4 for *LncBAR*$^{KO}$ brains. Cell counting was performed within frames [1120 µm (height)×560 µm (width)] spanning the entire cortex. (F) BrdU was administered at E13.5 and double-labeling of BrdU and CTIP2 was performed at P7. Outlined regions are enlarged on the right. (G) Quantification of BrdU$^+$ cells in I. *n*=5 for wild-type brains and *n*=5 for *LncBAR*$^{KO}$ brains. (H) Neocortices shown in F were divided into 10 bins of equal height and fixed width, and BrdU$^+$ cells in each bin were counted and quantified. Each frame is 984 µm (h)×820 µm (w) and spans the entire cortical thickness. (I) BrdU was administered at E15.5 and double labeling of BrdU and SATB2 was performed at P7. Outlined regions are enlarged on the right and in insets. (J) Quantification of BrdU$^+$ cells in I. *n*=5 for wild-type brains and *n*=4 for *LncBAR*$^{KO}$ brains. (K) Neocortices shown in I were divided into 10 bins of equal height and fixed width, and BrdU$^+$ cells in each bin were counted and quantified. Each frame is 984 µm (h)×820 µm (w) and spans the entire cortical thickness. Data are mean±s.e.m. Statistical significance was determined using an unpaired two-tailed Student's *t*-test (C-E,G,J), Mann–Whitney test (B) or two-way ANOVA followed by Sidak's multiple comparisons test (H,K). **P*<0.05; ***P*<0.01; *****P*<0.0001; ns, not significant. I, layer I; II-IV, layer II-IV; V, layer V; VI, layer VI; WM, white matter.

OB cells were lower in *LncBAR*$^{KO}$ brains (Fig. 4F-I). Importantly, numbers of SOX2$^+$ cells in the V-SVZ of the walls of the lateral brain ventricles were significantly fewer in *LncBAR*$^{KO}$ brains (Fig. 4J-L and Fig. S5E) with unaltered dublecortin$^+$ neuroblast in the V-SVZ and RMS (Fig. S5I), indicating *LncBAR* ablation diminished the aNSC pool in the V-SVZ.

It has been reported that aNSCs are descendants of embryonic neural progenitors (Fuentealba et al., 2015; Furutachi et al., 2015). At E16.5, P0, P3 and P7, OB length and area were the same in control and *LncBAR*$^{KO}$ brains (Fig. S5J-Q). We therefore stained E16.5 embryonic brains for SOX2, the marker for neural progenitors, to reveal that the numbers of SOX2$^+$ progenitor cells in both dorsal and ventral telencephalons were significantly lower in *LncBAR*$^{KO}$ brains (Fig. 4M-P and Fig. S4F). In developing dorsal forebrains, SOX2 labels RGs but is absent in some PAX6$^+$TBR2$^+$ cells (Hutton and Pevny, 2011). In embryonic *LncBAR*$^{KO}$ cortices, numbers of PAX6$^+$TBR2$^+$ IPs are significantly increased (Fig. 2G) along with unaltered PAX6$^+$ cells (Fig. 2E), which aligned with fewer SOX2$^+$ cells upon loss of *LncBAR* (Fig. 4N). Consistently, the self-renewal capacity of E12.5 *LncBAR*$^{KO}$ neocortical NPCs cultured *in vitro* was also greatly compromised (Fig. S5R,R′). Loss of *LncBAR* leads to a shrunken aNSC pool due to diminished NPC pool during embryonic stages.

### *LncBAR* associates with the SWI/SNF complex to maintain expression of *Zbtb20*

We next dissected molecular programs underlying the role of *LncBAR* in controlling neocortical neurogenesis, particularly in regulating cell-cycle progression of IPs. As *LncBAR* is mostly localized to the nucleus (Fig. S1B), we reasoned that *LncBAR* might regulate transcription of key fate specifier(s) and/or cell-cycle regulators by associating with and modifying the transcriptional machinery. First, biotin-labeled sense and antisense *LncBAR* were *in vitro* transcribed to pull down nuclear extracts of E14.5 neocortices for mass-spectrum protein identification. Interestingly, multiple components of the SWI/SNF chromatin-remodeling complex, also known as the BAF complex, were identified, including BRG1/SMARCA4, BAF155/SMARCC1 and BAF250a/ARID1A/SMARCF1 (Fig. 5A and Fig. S6A). RNA pull-down experiments followed by immunoblotting confirmed stronger binding of sense *LncBAR* to BRG1, ARID1A and BAF155 when compared with the binding of antisense controls (Fig. 5B). RIP assay also showed that BRG1, the enzymatic component of the BAF complex, associates with *LncBAR* (Fig. 5C). However, loss of *LncBAR* has no effect on the expression of BAF components in E16.5 neocortex (Fig. S6B) and the association of BAF components with BRG1 was unaffected (Fig. S6C).

We noticed that knockout of *LncBAR* had no effect on the expression levels of its two neighboring genes: *Zfp207* and *Psmd11* (Fig. S6D). Thus, RNA-seq transcriptome analyses were performed using wild-type and *LncBAR*$^{KO}$ neocortical NPCs, which unveiled 177 and 223 transcripts were significantly down- and upregulated upon loss of *LncBAR* (Fig. S6E). In parallel, ChIP-seq analyses were carried out using the anti-BRG1 antibody. When combining ChIP-seq and RNA-seq data (Fig. 5D and Fig. S6F), the *Zbtb20* gene, a transcription factor gene with an essential role in cortical development and adult neurogenesis (Doeppner et al., 2019; Tonchev et al., 2016), was found to be downregulated but more strongly associated with BRG1 in *LncBAR*$^{KO}$ neocortical NPCs (Fig. 5E,E′). Notably, single-cell transcriptome data from mouse and human developing neocortex showed expression patterns of BAF components and *Zbtb20* are mutually exclusive, with human *ZBTB20* displaying relative lower expression than mouse *Zbtb20* in IPs and PNs (Fig. S6G). Immunoblotting verified the decreased ZBTB20 expression in E16.5 *LncBAR*$^{KO}$ neocortices (Fig. 5F). Thus, depletion of *LncBAR* enhances the association of the BAF complex with *Zbtb20* gene, leading to its repression. The absence of *LncBAR* and higher expression of BRG1/SMARCA4 might account for restricted expression of *ZBTB20* in human embryonic neocortex.

### ZBTB20 expression enhances cell cycle progression of IPs of the *LncBAR*$^{KO}$ neocortex

We next examined whether overexpressing ZBTB20 could enhance cell cycle progression of *LncBAR*$^{KO}$ IPs. Plasmids expressing full-length ZBTB20 or zinc-finger-deleted ZBTB20 (ZBTB20-ΔZnf) were electroporated into E13.5 dorsal forebrains of *LncBAR*$^{KO}$ neocortices (Fig. 6A and Fig. S7A). ZBTB20-ΔZnf abolished the exclusively nuclear localization of ZBTB20 and showed defects in regulating dendritic arborization of neocortical neurons (Jones et al., 2018). Immunostaining showed overexpressed ZBTB20 was largely nuclear localized, whereas ZBTB20-ΔZnf was mostly cytosolic with a fraction also in nuclei (Fig. S7B). Significantly fewer ZBTB20-expressing cortical cells migrated to the cortical plate (Fig. 6B,C). BrdU was injected at E15.5, and E16.5 embryos were collected for co-labeling studies (Fig. 6D,E). Significantly more ZBTB20-expressing cortical cells were actively cycling, as more ZBTB20-expressing cells were double positive for Ki67 and BrdU (24 h) (Fig. 6F,G). Specifically, more ZBTB20-transduced cells were TBR2$^+$ IPs (Fig. 6H) and more ZBTB20-expressing TBR2$^+$ IPs expressed Ki67 (Fig. 6I), indicating that ZBTB20 expression reversed the delayed cell cycle of IPs caused by *LncBAR* deletion. Intriguingly, expression of ZBTB20-ΔZnf had minor effects on cell proliferation, suggesting a transcription-dependent role for ZBTB20 in maintaining IP divisions or a residual transactivating effect of ZBTB20-ΔZnf.

### *LncBAR* overexpression promotes the NPC fate and IP divisions

We finally applied *in utero* electroporation to explore whether overexpression of *LncBAR* could promote the NPC fate and IP divisions. Indeed, a larger proportion of *LncBAR*-overexpressing neocortical cells resided in the VZ/SVZ region and expressed SOX2, but fewer had migrated into the cortical plate (Fig. 7A-C).

Development (2021) 148, dev199772. doi:10.1242/dev.199772

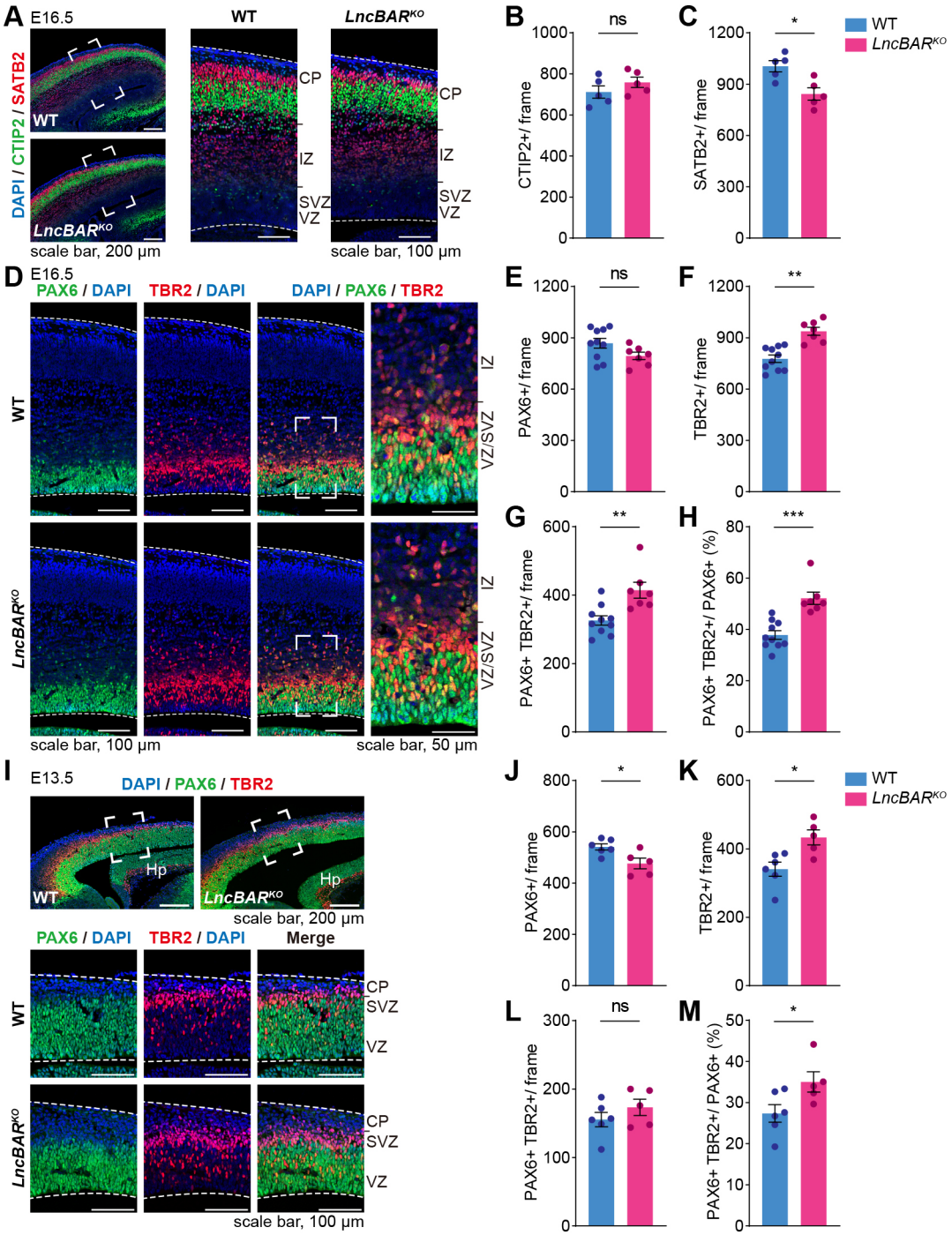


**Fig. 2. Expanded IP pool in *LncBAR*$^{KO}$ neocortex.** (A) Double immunofluorescence of CTIP2 (green) and SATB2 (red) on coronal sections of E16.5 wild-type and *LncBAR*$^{KO}$ neocortices. Nuclei were labeled with DAPI (blue). Outlined regions are enlarged on the right. (B,C) Quantification of CTIP2$^{+}$ (B) and SATB2$^{+}$ (C) cells at E16.5. Cell counting was performed within frames [664 µm (h)×322 µm (w)] spanning the neocortex. *n*=5 for wild-type brains and *n*=5 for *LncBAR*$^{KO}$ brains. (D) Double immunofluorescence of PAX6 (green) and TBR2 (red) on coronal sections of E16.5 wild-type and *LncBAR*$^{KO}$ cortices. Nuclei were stained with DAPI (blue). (E-H) Quantification of PAX6$^{+}$ cells (E), TBR2$^{+}$ cells (F), PAX6$^{+}$TBR2$^{+}$ double-positive cells (G) and PAX6$^{+}$/TBR2$^{+}$ cells relative to PAX6$^{+}$ cells (H) at E16.5. Cell counting was performed with frames [664 µm (h)×322 µm (w)] spanning the neocortex. *n*=10 for wild-type brains and *n*=7 for *LncBAR*$^{KO}$ brains. (I) Double immunofluorescence of PAX6 (green) and TBR2 (red) on coronal sections of E13.5 wild-type and *LncBAR*$^{KO}$ neocortices. Outlined regions are enlarged on the right. Nuclei were labeled with DAPI (blue). (J-M) Quantification of PAX6$^{+}$ cells (J), TBR2$^{+}$ cells (K), PAX6$^{+}$TBR2$^{+}$ double-positive cells (L) and PAX6$^{+}$/TBR2$^{+}$ cells relative to PAX6$^{+}$ cells (M) at E13.5. Cell counting was performed within frames [299 µm (h)×249 µm (w)] spanning the cortex. *n*=6 for wild-type brains and *n*=5 for *LncBAR*$^{KO}$ brains. Data are mean±s.e.m. Statistical significance was determined using an unpaired two-tailed Student's *t*-test (B,C,E-G,J-M) or Mann–Whitney test (H). *$P$<0.05; **$P$<0.01; ***$P$<0.001; ns, not significant. VZ, ventricular zone; SVZ, subventricular zone; IZ, intermediate zone; CP, cortical plate.

Furthermore, significantly more *LncBAR*-overexpressing cells, particularly TBR2$^{+}$ IPs, were actively cycling: more *LncBAR*-overexpressing cells expressed Ki67 and more transduced TBR2$^{+}$ IPs expressed Ki67 (Fig. 7D-G). In summary, *LncBAR* acts *in trans* to temporally regulate the NPC fate, IP divisions and, hence, neurogenesis during neocortical development.

Development (2021) 148, dev199772. doi:10.1242/dev.199772

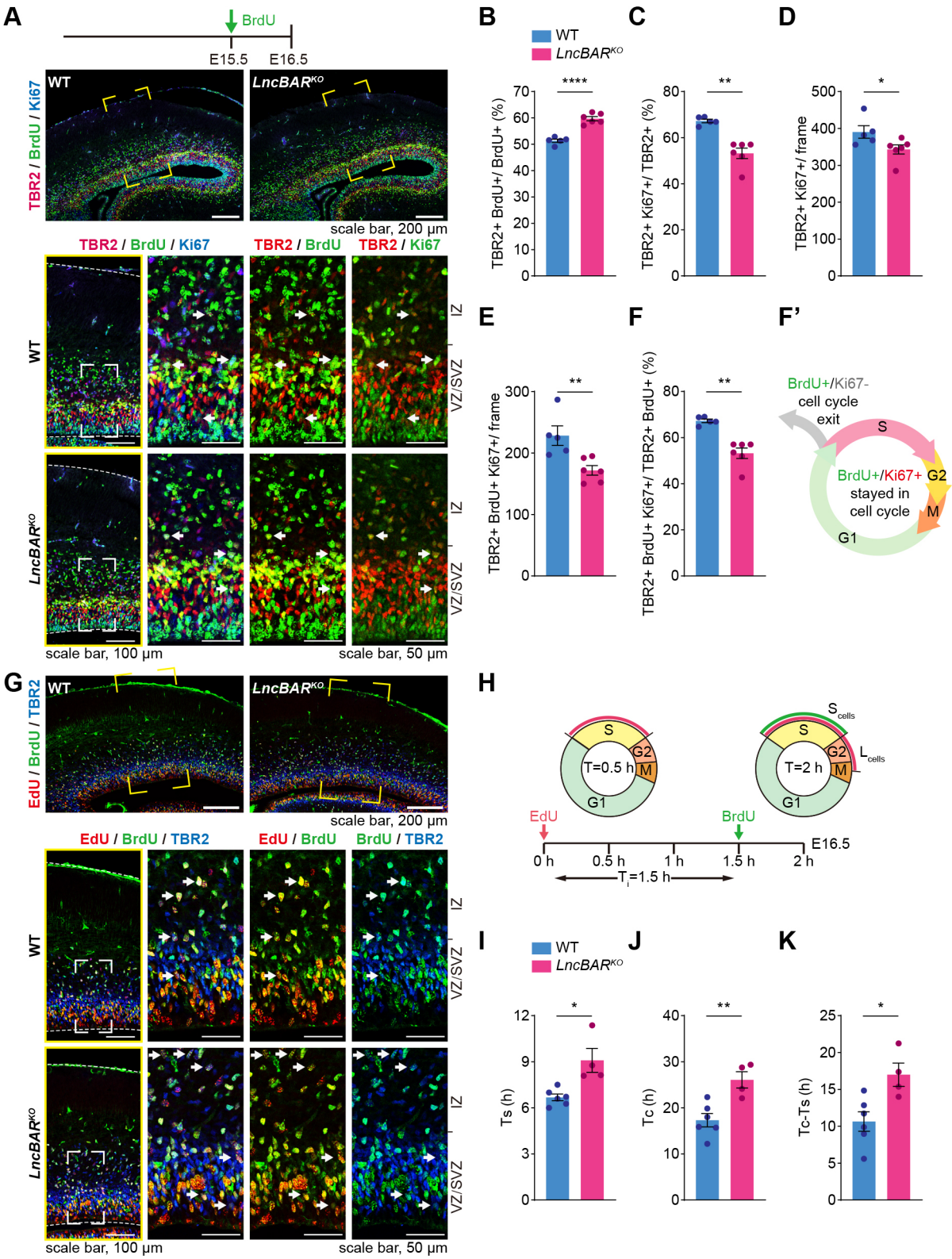


**Fig. 3.** See next page for legend.

## DISCUSSION

Neuronal production and neocortex size are determined, to a significant extent, by the abundance and proliferative capacity of neural progenitors, including RGs and IPs, during development. Indirect neurogenesis, i.e. RGs→IPs→PNs, is predominant in neocortex development of both rodents and primates (Franco and Müller, 2013). Specifically, primates increase the neurogenic NPC pool size by using symmetric proliferative divisions of basal progenitors, including both bRGs and bIPs (Florio and Huttner, 2014; Haubensak et al., 2004; Martinez-Cerdeno et al., 2006;

Development (2021) 148, dev199772. doi:10.1242/dev.199772

**Fig. 3. Lengthened IP cell cycle upon loss of *LncBAR*.** (A) BrdU was administrated at E15.5 and triple labeling of TBR2, BrdU and Ki67 was performed on E16.5 neocortical sections. Outlined regions are enlarged underneath. Arrows indicate TBR2$^+$BrdU$^+$Ki67$^+$ cells. (B-F) Quantification of data in A: TBR2$^+$BrdU$^+$cells relative to BrdU$^+$ cells (B); TBR2$^+$Ki67$^+$ cells relative to TBR2$^+$ cells (C); numbers of TBR2$^+$Ki67$^+$ cells per frame (D); numbers of TBR2$^+$BrdU$^+$Ki67$^+$ cells per frame (E); TBR2$^+$BrdU$^+$Ki67$^+$ cells relative of TBR2$^+$BrdU$^+$ cells (F). *n*=5 for wild-type brains and *n*=6 for *LncBAR*$^{KO}$ brains. (F′) Schematic illustration of cell cycle exit. BrdU$^+$Ki67$^+$ cells represent cells that remained in the cell cycle; BrdU$^+$/Ki67$^-$ cells represents cells that have exited the cell cycle. (G) Triple-labeling of TBR2, EdU and BrdU on E16.5 wild-type and *LncBAR*$^{KO}$ cortices, as labeled in H. Outlined regions are enlarged underneath. Arrows indicate TBR2$^+$EdU$^+$BrdU$^+$ cells. (H) Schematic illustration of cell-cycle length measurements using sequential EdU/BrdU labeling. (I-K) Periods of S-phase (Ts) (I), cell cycle length (Tc) (J) and Tc-Ts (K). Cell counting was performed within frames [664 µm (h)×322 µm (w)] spanning the cortex. *n*=6 for wild-type brains and *n*=4 for *LncBAR*$^{KO}$ brains. Data are mean±s.e.m. Statistical significance was determined using an unpaired two-tailed Student's *t*-test (B,D,E,J,K), a Student's two-tailed unpaired *t*-test with Welch's correction (I) or a Mann–Whitney test (C,F). **P*<0.05; ***P*<0.01; *****P*<0.0001. VZ, ventricular zone; SVZ, subventricular zone; IZ, intermediate zone.

Sessa et al., 2008). Another important factor concerning expansions of primate neocortex is the lengthening of neurogenic time windows, from days in rodents to months in primates (Dehay and Kennedy, 2007; Garcia et al., 2016; Lui et al., 2011). Moreover, fate commitment of neural progenitors is closely related to and may be the consequence of the pace of cell cycle progression (Calegari et al., 2005; Lange and Calegari, 2010; Orford and Scadden, 2008; Salomoni and Calegari, 2010; Singh and Dalton, 2009). Therefore, coordinating neurogenesis with cell cycle progression of IPs, both in frequencies and time frames, is quintessential for neocortex expansion during development and in evolution (Lim and Kaldis, 2012).

Here, we revealed that *LncBAR*, a BAF chromatin-remodeling complex associated long non-coding RNA, plays essential roles in abundance and cell cycle progression of IPs. Loss of *LncBAR* causes excessive IPs in the SVZ, while the proliferative capacity of IPs was greatly compromised in mid-late neurogenesis. As a result, *LncBAR* knockout neocortices have more deep-layer but fewer upper-layer PNs (Fig. 7H). The disproportionate cortical layering and IP accumulation reported here is reminiscent of some phenotypes caused by loss of ATRX, a SWI/SNF2-type chromatin remodeling protein associated with pericentromeric and telomeric heterochromatin, in developing forebrain (Ritchie et al., 2014). However, unlike the transcriptional regulation of *Zbtb20* by the BAF/LncBAR complex, ATRX is believed to control cell cycle progression by regulating mitotic spindle angles and ensuring proper chromosome congression and segregation of neocortical progenitors (Ritchie et al., 2008, 2014). Mechanistically, *LncBAR* functions as a 'decoy' to block the association of the BAF chromatin-remodeling complex with the genomic region of *Zbtb20*, thus allowing its expression (Fig. 7H). In the absence of *LncBAR*, more BAF complex associates with the *Zbtb20* gene to inhibit its transcription. A number of studies also revealed that binding of the BAF complex, particularly BRG1, to nuclear factors or to LncRNAs could modulate the target gene association and transcription activities of BAF to specify cell fates in accordance with spatiotemporal requirements (Cajigas et al., 2015; Han et al., 2014; Lino Cardenas et al., 2018; Seo et al., 2005; Wang et al., 2015). We did not detect compositional alterations of major BAF components upon loss of *LncBAR*. However, given ubiquitous expression of *LncBAR* in developing neocortex, it deserves to extensively dissect dynamics of BAF components and target gene expressions in RGs, IPs and PNs with or without *LncBAR*.

The BAF complex plays key roles in neocortical neurogenesis by regulating a plethora of transcriptional programs and cell-cycle progression of NPCs (Sokpor et al., 2018). Cell cycle exit and differentiation of NPCs coincides with BAF subunit swap to produce neuron-specific BAF (nBAF) complexes (Braun et al., 2021; Lessard et al., 2007; Staahl et al., 2013). Loss of distinct subunits of the BAF complex showed variable alteration of neocortical development, abundance and distributions of IPs, reflecting the complex dynamics of and causal relationships between BAF compositions, genomic association and target gene regulations (Braun et al., 2021; Narayanan et al., 2018, 2015; Nguyen et al., 2018; Tuoc et al., 2013). Notably, loss of BAF53a stalls the cell cycle of RGs and IPs at G2/M to disrupt neocortical neurogenesis with an increase of PAX6$^+$ and TBR2$^+$ co-expression, which partially resembles defects of *LncBAR*$^{KO}$ neocortices (Braun et al., 2021). Molecularly, BAF53a ablation leads to reduced chromatin accessibility at neurogenesis transcription factor-binding sites, perhaps due to Polycomb enrichment. Decreased expression of *Zbtb20* in *LncBAR*$^{KO}$ NPCs could be caused by altered chromatin accessibility and the status of Polycomb-mediated repression, which deserve further exploration.

Although knockout of *Baf170* causes overproduction of neocortical PNs, *Baf155*/*Baf170* conditional double-knockout results in significant decrease of upper-layer neurons, as well as aplasia of hippocampus, the latter of which was marked by diminished expression of ZBTB20 (Nguyen et al., 2018). As a temporal regulator, ZBTB20 has important functions in cortical layer formation, neurogenesis of the OB and the hippocampus, and gliogenesis, depending on the developmental context (Doeppner et al., 2019; Nielsen et al., 2010, 2007; Tonchev et al., 2016; Xie et al., 2010). Loss of *Zbtb20* in mice results in compromised upper-layer formation and a smaller OB, reminiscent of *LncBAR*$^{KO}$ brains (Doeppner et al., 2019; Tonchev et al., 2016). In addition, proliferative potentials of *LncBAR*$^{KO}$ IPs were hampered in mid-late but not in early neurogenesis, which coincides with incremental expression levels of *Zbtb20* over the period of neocortical development (Tonchev et al., 2016). Importantly, our studies showed that overexpression of full-length ZBTB20 but not the zinc-finger-deleted ZBTB20-ΔZnf could enhance IP proliferation in *LncBAR*$^{KO}$ neocortices. Thus, *LncBAR* provides an essential molecular cog that links the BAF complex with the transcriptional control of *Zbtb20* to temporally control cell cycle progressions and fate choices of IPs.

Loss of *LncBAR* also causes a reduced NSC pool in the adult V-SVZ and fewer OB interneurons, probably due to exhausted embryonic NPCs. *In vitro* neurosphere studies indeed showed that the self-renewal capacity of *LncBAR*$^{KO}$ NPCs was greatly compromised, which is in line with a decreased number of SOX2$^+$ NPCs in both dorsal and ventral *LncBAR*$^{KO}$ forebrains. It remains to be studied whether *LncBAR* could modulate cell cycle progression and differentiation of the aNSC lineage. Finally, *LncBAR* is present in mice but not in primates. We speculate that the absence of *LncBAR* and relative lower expression of ZBTB20 in developing primate neocortex could lengthen the cell cycle period of IPs, which might be one of the mechanisms that prolong neurogenic time to facilitate neocortical expansion in primate brains.

## MATERIALS AND METHODS

### Animals and genotyping

All animal procedures were approved by the Animal Care and Ethical Committee of College of Life Sciences and Medical Research Institute at

Development (2021) 148, dev199772. doi:10.1242/dev.199772

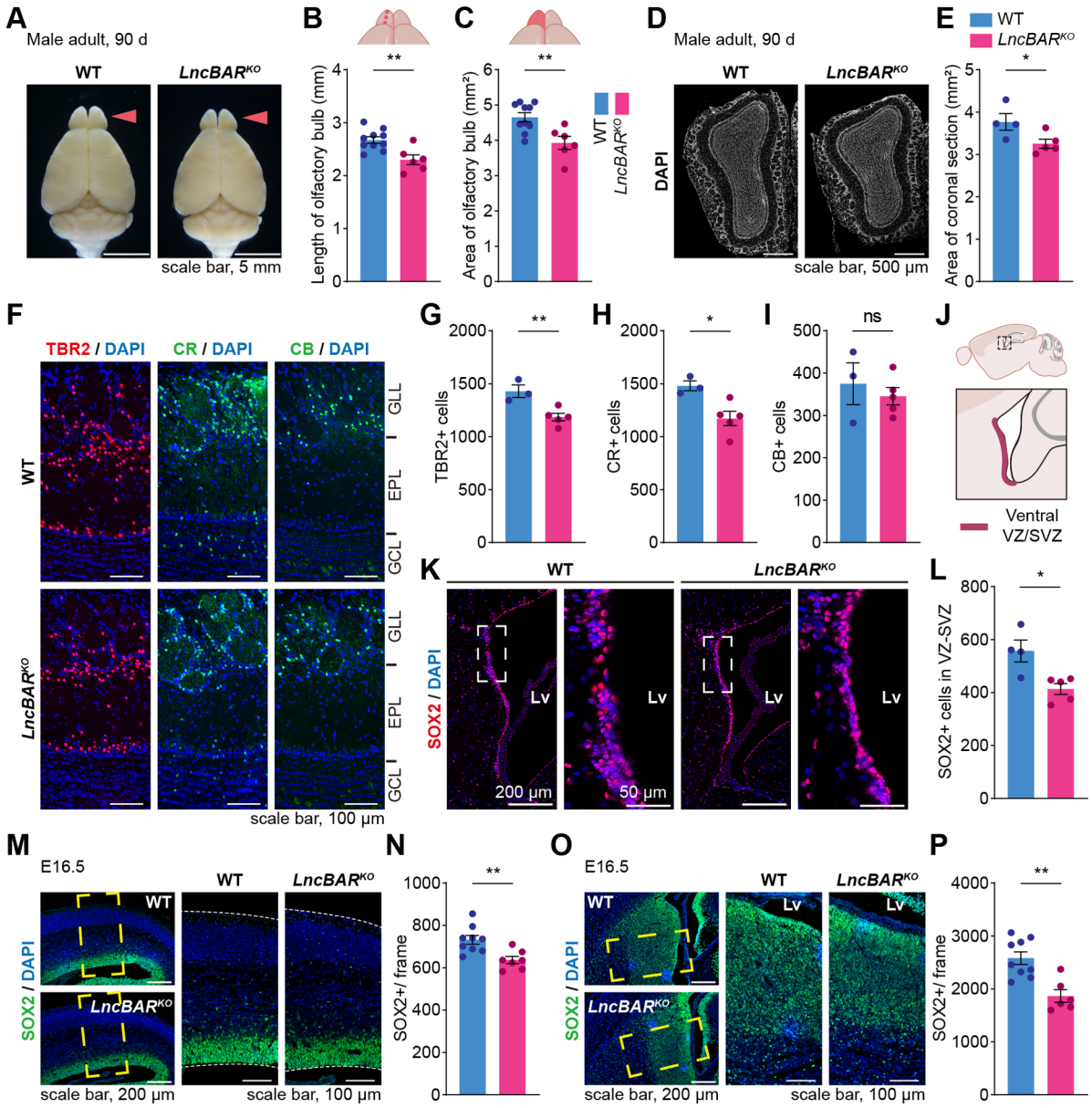


**Fig. 4. Smaller olfactory bulbs and a compromised NSC pool in *LncBAR*$^{KO}$ brains.** (A-C) Representative images of male adult wild-type and *LncBAR*$^{KO}$ brains (A), and measurements of length and area of olfactory bulb (OB) hemispheres (B,C). *n*=10 for wild-type mice and *n*=6 for *LncBAR*$^{KO}$ brains. (D,E) Representative DAPI staining of OB coronal sections in male adult mice (D) and quantifications of the OB area (E). *n*=4 for wild-type brains and *n*=5 for *LncBAR*$^{KO}$ brains. (F-I) Immunofluorescent staining (F) and quantifications of TBR2$^{+}$ (G), calretinin$^{+}$ (CR) (H) and calbindin$^{+}$ (CB) (I) cells in OBs. Nuclei were labeled with DAPI (blue). *n*=3 for wild-type brains and *n*=5 for *LncBAR*$^{KO}$ brains. Cell counting was performed within frames [664 µm (h)×322 µm (w)] spanning the neocortex. (J) Schematic diagram showing VZ-SVZ in the adult brain. (K,L) Representative fluorescence images (K) and quantifications (L) of SOX2$^{+}$ cells in VZ-SVZ. Nuclei were labeled with DAPI (blue). *n*=4 for wild-type brains and *n*=5 for *LncBAR*$^{KO}$ brains. (M-P) Representative fluorescence images and quantifications of SOX2 in dorsal (M,N) and ventral (O,P) forebrains at E16.5. Nuclei were labeled with DAPI (blue). Outlined regions are enlarged on the right. *n*=9 for wild-type brains and *n*=7 for *LncBAR*$^{KO}$ brains in N; *n*=9 for wild-type brains and *n*=6 for *LncBAR*$^{KO}$ brains in R. Counting of SOX2$^{+}$ cells was performed within frames [664 µm (h)×322 µm (w)]. Data are mean±s.e.m. Statistical significance was determined using an unpaired two-tailed Student's *t*-test (B,C,E,G-I,L,N,P). **P*<0.05; ***P*<0.01; ns, not significant. VZ, ventricular zone; SVZ, subventricular zone; Lv, lateral ventricle; GLL, glomerular layer; EPL, external plexiform layer; GCL, granule cell layer.

Wuhan University. Wild-type CD-1 and C57BL/6 mice were obtained from the Hunan SJA Laboratory Animal Company (Changsha, China). *LncBAR*$^{+/-}$ mice were generated by Biocytogen (Beijing, China) using the CRISPR/Cas9-mediated gene editing. Two sgRNAs were designed to generate a chromosomal deletion at the intergenic region located between *Zfp207* and *Psmd11* in the mouse genome. For cloning the sgRNA-expression cassette, annealed DNA was ligated to pT7-sgRNA-2G and confirmed by DNA sequencing. Targeting vector, Cas9 vector and sgRNAs were microinjected into mouse zygotes. Zygotes were transferred into pseudo-pregnant female mice to generate founders, which were genotyped by PCR and sequencing. Positive founders were crossed with C57BL/6 wild-type mice to generate F1 mice. The primer set for genotyping is: wild-type and KO forward, 5′-TTG TCC AGC AAT CAC AAC TGC CTGT-3′; wild-type reverse, 5′-AGC ACA CTG TCT CTG CCT CTT GG-3′; KO reverse, 5′-TGT GCT GTT CTC GGG AGA GTT AGG A-3′. Band sizes for the wild-type allele and KO allele are 685 bp and 554 bp, respectively. The day when a vaginal plug was detected was counted as embryonic (E) day 0.5.

Development (2021) 148, dev199772. doi:10.1242/dev.199772

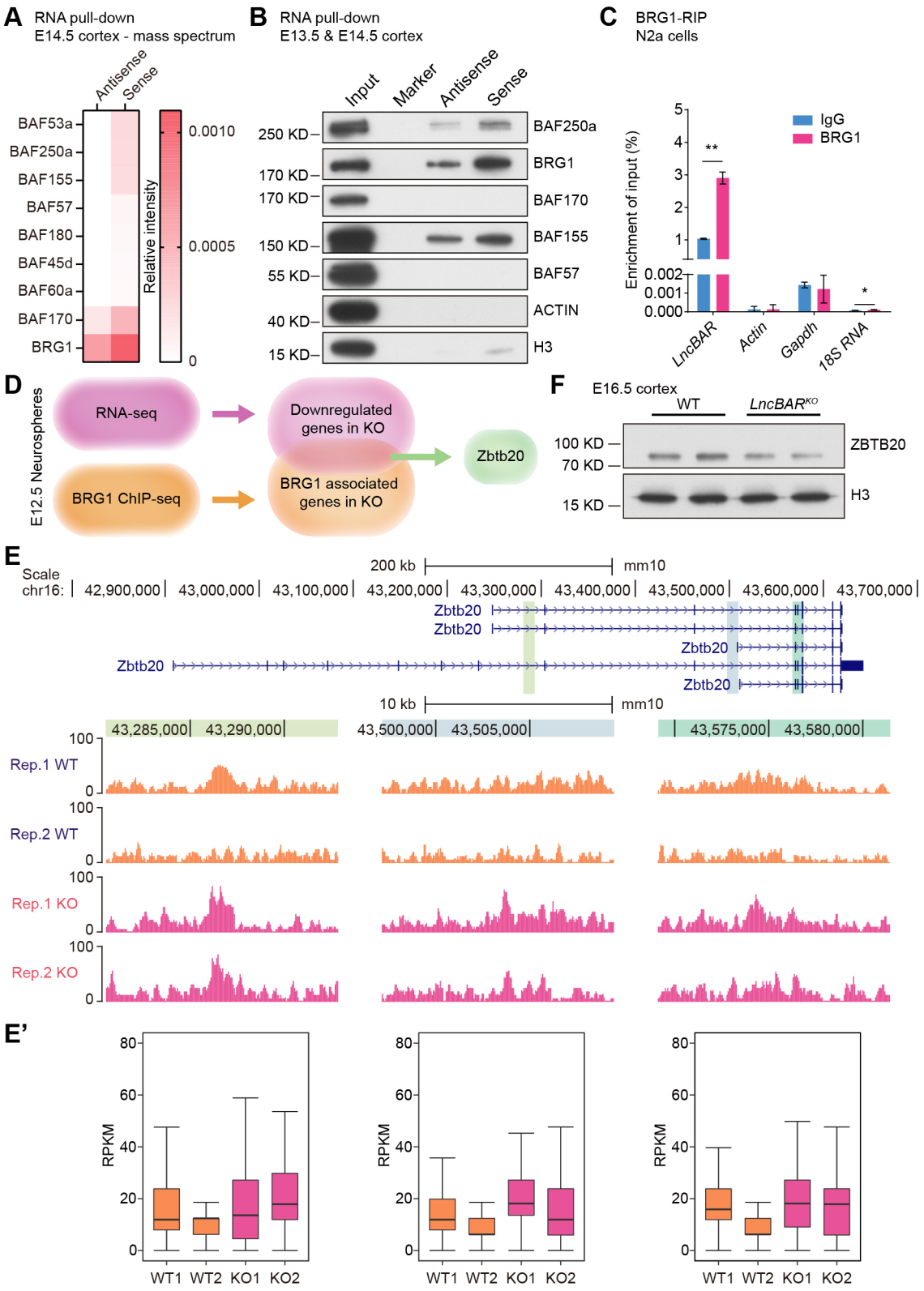


**Fig. 5.** See next page for legend.

## Cell cultures

Neuro-2a cells were purchased from the Cell Bank of Chinese Academy of Sciences Cells and maintained in indicated culture media (MEM) containing 10% fetal bovine serum (Life Technologies or Hyclone). Only cells within ten passages were used. For neurosphere culture assays, cortical NPCs dissociated from E12.5 mouse cortex were cultured on ultra-low-attachment 6-well plates (Corning) and maintained in F12 medium (Life Technologies) at $6\times10^4$ cells/ml with N2 and B27 supplements (Life Technologies), 1 mmol/l N-acetyl-L-cysteine (NAC), and human recombinant FGF2 and EGF (20 ng/ml each; Life Technologies) for 6~7 days. Neurospheres were dissociated enzymatically into single cells and cultured for ~6-7 days for each passage. Numbers of cells were analyzed after three passages (Luo et al., 2020).

Development (2021) 148, dev199772. doi:10.1242/dev.199772

**Fig. 5. *LncBAR* associates with the BAF complex to maintain the expression of *Zbtb20*.** (A) RNA pull-down assay was performed using nuclear extracts of E14.5 neocortices followed by mass spectrometry. Multiple components of the BAF complex were enriched in *LncBAR*-precipitated extracts compared with those precipitated by antisense *LncBAR*. Heatmap showed quantitative proteome profiles. Relative intensities are shown as enrichment ratios of differentially precipitated proteins in total precipitated proteome profiles (refer to Table S1 for more details). (B) Immunoblots of BAF components associated with sense or antisense *LncBAR* using extracts of E13.5 and E14.5 neocortices. (C) RNA immunoprecipitation (RIP) of anti-BRG1 and control IgG antibodies followed by RT-qPCR analyses using extracts of Neuro-2a cells. (D) Schematic illustration showing integration of RNA-seq with the anti-BRG1 ChIP-seq data to identify target gene(s) regulated by the BRG1/*LncBAR* complex. (E) The anti-BRG1 ChIP-seq studies showing association of BRG1 with three genomic regions of *Zbtb20* in wild-type and *LncBAR*$^{KO}$ neocortical neurospheres. Colored regions at the top are shown in more detail underneath. (E′) Boxplots showing the ChIP-seq signals (RPKM) of BRG1 in the three regions (region center±3 kb). RPKM was calculated by deeptools (v3.5.1). The box represents the lower quartile, the median (bold line inside the box) and the upper quartile. IQR (interquartile range) is the distance between the upper and lower quartiles. Whiskers indicate 1.5 times the IQR ranges. (F) Immunoblots of ZBTB20 and H3 using extracts of E16.5 wild-type and KO neocortices. In C, data are mean±s.d. Statistical significance was determined using Student's two-tailed unpaired *t*-test (for *Actin*, *Gapdh* and *18S RNA*) or Student's two-tailed unpaired *t*-test with Welch's correction (for *LncBAR*). **P*<0.05; ***P*<0.01.

### 5′ and 3′ rapid amplification of cDNA ends (5′ and 3′ RACE)

Nested primers were synthesized according to the *LncBAR* sequence as described in previous studies (Okazaki et al., 2002; Tian et al., 2021). For 5′ and 3′ RACE, a SMART RACE Kit (Clontech) was applied according to the manufacturer's guide. PCR products were cloned into pGEM-T easy vectors (Promega) and analyzed by Sanger sequencing to identify the 5′ and 3′ ends of *LncBAR*. The primers used are listed in Table S3.

### Northern blot

RNA fractionation was performed as previously described (Tian et al., 2021). Total RNA was extracted using the RNAiso Plus solution (Takara) from Neuro-2a cells. Total RNA from Neuro-2a cells (20 µg) and 1 µg of pCAGGS-*LncBAR* transduced Neuro-2a cells were subjected to formaldehyde denaturing agarose electrophoresis. Subsequently, RNA samples were transferred to a positively charged nylon membrane (Beyotime) with 20×SSC buffer (3.0 mol/l NaCl and 0.3 mol/l sodium citrate, pH 7.0) through an ascending capillary transfer system. Wet membranes were cross-linked by UV irradiation (254 nm for 1 min 45 s, 1.5 J/cm$^2$) and incubated with pre-warmed DIG Easy Hyb Hybridization solution (Roche) at 65°C for 1 h pre-hybridization. DIG-labeled RNA probes (*LncBAR* and *Gapdh*) generated by *in vitro* transcription were denatured at 85°C for 5 min and chilled on ice. Membranes were then incubated with DIG-labeled RNA probes and hybridization was carried out overnight at 65°C. Membranes were stringently washed three times in wash buffer 1 (0.1× SSC and 0.1% SDS) for 15 min at 65°C, then rinsed in wash buffer 2 [0.1 mol/l maleic acid, 0.15 mol/l NaCl and 0.3% Tween 20 (pH 7.5)] and incubated in blocking reagent (Roche) for 1 h at room temperature. After incubation, the membrane was incubated with a 50,000-fold dilution of anti-DIG-AP Fab fragment (Roche) in blocking reagent for 30 min at room temperature, and washed three times in wash buffer 2 (each for 10 min) at room temperature. After washing, the membrane was immersed in detection buffer [0.1 mol/l Tris-HCl, 0.1 mol/l NaCl (pH 9.5)] for 5 min and anti-DIG-AP was detected using CDP-star chemiluminescent substrate for alkaline phosphatase (Roche) and X-ray film exposure. The primers used are listed in Table S3.

### RNA fractionation

RNA fractionation was performed as previously described (Cabianca et al., 2012). In brief, neural progenitor cells from E12.5 mouse cortices were detached by treating with papain, counted and centrifuged at 168 ***g*** for 5 min. The pellet was lysed with 175 µl/10$^6$ cells of cold RLN1 solution [50 mmol/l Tris-HCl (pH 8.0), 140 mmol/l NaCl, 1.5 mmol/l $MgCl_2$, 0.5% NP-40, 2 mmol/l vanadyl ribonucleoside complex (Sangon Biotech)] for 5 min. The suspension was centrifuged at 4°C and 300 ***g*** for 2 min. The supernatant, corresponding to the cytoplasmic fraction, was transferred into a new tube and stored on ice. The pellet containing nuclei was corresponding to nuclear fractions. Total RNA was extracted from the cytoplasmic and nuclear fractions using RNAiso Plus solution (Takara). Samples were treated with DNase I, washed with 70% ethanol and then resolved in 30 µl RNase-free water. RNA (1 µg) was used for the first-strand synthesis with the PrimerScript Reverse Transcriptase (Takara) using oligo-dT and random primers. The cDNA was then subjected to qRT-PCR using the SYBR Green assay with 2× SYBR Green qPCR master mix (Bimake), and analyzed by a CFX Connect Real-Time PCR Detection System (Bio-rad). The primers used are listed in Table S3.

### Real-time quantitative reverse transcription PCR (qRT-PCR)

Total RNAs (0.5-1 µg) were reverse transcribed at 42°C using PrimerScript Reverse Transcriptase (Takara). 2× SYBR Green qPCR master mix (Bimake) was then applied to perform quantitative PCR on a CFX Connect Real-Time PCR Detection System (Bio-rad). The thermal profile was 95°C for 5 min and 40 cycles of 95°C for 15 s and 60°C for 20 s. Relative gene expression was determined using the $2^{-\Delta\Delta Ct}$ method, normalizing to housekeeping genes *Gapdh*. The primers used are listed in Table S3.

### Tissue fixation and sectioning

Pregnant mice were deeply anesthetized with 0.7% (w/v) pentobarbital sodium (10$^5$ mg/kg of body weight) in 0.9% sodium chloride before sacrifice. Embryos were then removed from the uteri rapidly. Embryonic brains were dissected in ice-cold phosphate-buffered saline (PBS) and immersed in 4% paraformaldehyde (PFA) overnight at 4°C. P0, P7 and adult mice were deeply anesthetized with 0.7% (w/v) pentobarbital sodium solution followed by transcardiac perfusion with ice-cold 4% PFA in PBS. Brains were dissected and postfixed in 4% PFA overnight at 4°C. Fixation of embryonic and neonatal brains was followed by treatment of 20% sucrose in 1× PBS overnight at 4°C. For dehydration of adult brains, gradient sucrose solutions were used (20% and 30% sucrose in 1× PBS; each for 1 day, at 4°C). Tissues were embedded in Tissue-Tek OCT Compound (Sakura) and cryosections (14 µm for embryonic and neonatal brains, 20 µm for adult brains) were cut onto slides using a Leica CM1950 cryostat.

### Nissl staining

Adult brain sections were stained with 0.25% Cresyl Violet (Sigma-Aldrich) solution for 15 min at 65°C. Sections were then decolorized in ethanol for 0.5-1 min, dehydrated in ethanol for 5 min and cleared twice in xylene for 5 min. Sections were mounted in neutral balsam.

### *In situ* hybridization

*In situ* hybridization was performed as previously described (Li et al., 2017). Digoxigenin-labeled riboprobes were transcribed using the DIG-RNA Labeling Mix (Roche). Sections were dried in a hybridization oven at 50°C for 15 min and fixed in 4% PFA for 20 min at room temperature. Permeabilization was performed by using proteinase K (2 µg/ml) in PBS for 10 min at room temperature. Before hybridization, sections were acylated in 0.1 mol/l TEA (triethanolamine) solutions (10 ml 1 mol/l TEA solution and 250 µl acetic anhydride in 90 ml DEPC-treated deionized $H_2O$) for 10 min. Sections were then incubated with digoxigenin-labeled probes diluted (0.1∼0.2 ng/µl) in hybridization buffer [50% deionized formamide, 5× SSC, 5× Denhardt's, transfer RNA (tRNA) (250 µg/ml) and herring sperm DNA (500 µg/ml)] under coverslips in a hybridization oven overnight at 65°C. The next day, sections were washed four times, each for 20 min in 0.2× SSC at 65°C. Subsequently, they were treated with ribonuclease (RNase) A (20 µg/ml) for 20 min at 37°C and then blocked for 3-4 h at room temperature in 10% heat-inactivated normal sheep serum in buffer B1 [0.1 mol/l Tris-HCl (pH 7.4) and 150 mmol/l NaCl]. Slides were incubated with a 1:5000 dilution of anti-digoxigenin-AP Fab fragments from sheep (Roche) overnight at 4°C. After washing three times in buffer B1, sections

Development (2021) 148, dev199772. doi:10.1242/dev.199772

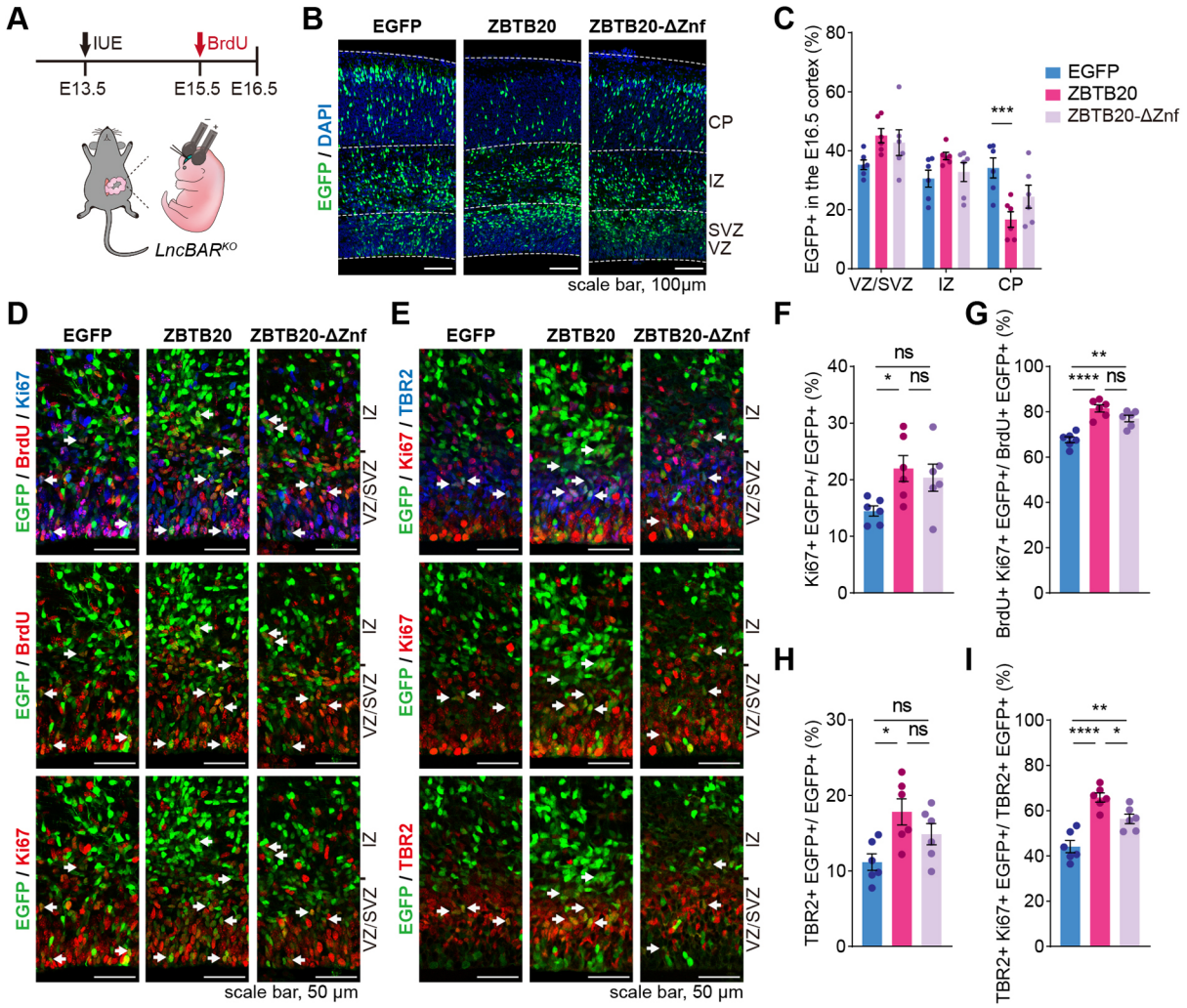


**Fig. 6. *Zbtb20* overexpression promotes IP proliferation in *LncBAR*$^{KO}$ neocortices.** (A) Schematic diagram illustrating the strategy of *in utero* electroporation (IUE) and BrdU injection of *LncBAR*$^{KO}$ embryos. (B) Representative images showing E16.5 neocortex transduced with indicated constructs with transduced cells labeled with EGFP. Nuclei were labeled with DAPI (blue). (C) Quantification of localization of EGFP$^+$ transduced cells in E16.5 neocortices. *n*=6 for EGFP, *n*=6 for ZBTB20 and *n*=6 for ZBTB20-ΔZnf. (D,E) Representative immunofluorescent images showing expression of BrdU$^+$/Ki67$^+$ (D) and Ki67$^+$/TBR2$^+$ (E) in EGFP$^+$ transduced cells at VZ/SVZ-IZ regions. Arrows indicate GFP$^+$/BrdU$^+$/Ki67$^+$ (D) and GFP$^+$/Ki67$^+$/TBR2$^+$ (E) cells. (F-I) Quantifications of Ki67$^+$EGFP$^+$/EGFP$^+$ (F), BrdU$^+$Ki67$^+$EGFP$^+$/BrdU$^+$EGFP$^+$ (G), TBR2$^+$EGFP$^+$/EGFP$^+$ (H) and TBR2$^+$Ki67$^+$EGFP$^+$/TBR2$^+$EGFP$^+$ (I) cells. *n*=6 for EGFP, *n*=6 for ZBTB20 and *n*=6 for ZBTB20-ΔZnf. Cell counting was performed within frames [830 μm (h)×415 μm (w)] and quantification data are shown as mean±s.e.m. In C, statistical significance was determined using two-way ANOVA followed by Tukey's multiple comparisons test. In F-I, statistical significance was determined using one-way ANOVA with Tukey's post-hoc tests. *$P$<0.05; **$P$<0.01; ***$P$<0.001; ****$P$<0.0001. ns, not significant.

were equilibrated twice in buffer B3 [0.1 mol/l Tris-HCl; 0.1 mol/l NaCl; 50 mmol/l $MgCl_2$; 0.1% Tween-20 (pH 9.5)] for 10 min. BCIP/NBT (bromochloroindolyl phosphate/nitro blue tetrazolium) (Roche) was used as the color-developing agent. Slides were incubated with the color-developing agent at room temperature for 7 h in dark. Slides were then dehydrated using gradient ethanol and xylene sequentially, and mounted with neutral balsam.

### Single-molecule fluorescent *in situ* hybridization

To prepare tissue sections for single-molecule fluorescent *in situ* hybridization (smFISH), mouse embryonic brains were microdissected, fixed with 4% PFA for 24 h and then dehydrated with 20-30% DEPC-treated sucrose for 24 h. Subsequently, tissues were rapidly frozen on dry ice, embedded in OCT compound, cryosectioned at 18 μm and mounted onto SuperFrost Plus microscope slides. To detect the expression level of *LncBAR*, we designed probes (Table S3) and employed *in situ* hybridization chain reaction approach (Choi et al., 2018; Mu et al., 2021). In brief, tissue sections were permeabilized in 70% ethanol for 16 h at 4°C, treated with 0.5% Triton X-100 in 1×PBS at 37°C for 1 h and then 10 μg/ml Protease K for 10 min. After two washes with 1×PBS at room temperature, sections were pre-hybridized in hybridization buffer (30% formamide, 5×SSC, 9 mM citric acid, 0.1% tween 20, 50 μg/ml heparin, 1×Denhardt's solution and 10% dextran sulfate) for 1 h at 37°C and then incubated with HCR probes (10 μM for each) for 3 h at 37°C. After mRNA hybridization, the signals were amplified by fluorescently labeled hairpins overnight at room temperature, followed by three washes with 5×SSCT buffer [0.75 M NaCl, 75 mM sodium citrate and 0.1% Tween 20 (pH=7)] before mounting.

### Immunofluorescence

Frozen brain sections were mounted onto Superfrost plus slides and then dried at room temperature. For heat-mediated antigen retrieval, slides were incubated for 15 min in 10 mM sodium citrate buffer (pH 6.0) at 95°C. For BrdU staining, sections were treated with 20 μg/ml proteinase K (Sigma) (1:1000 in PBC) for 5 min and 2 N HCl for 30 min at room temperature. Sections were then immersed in blocking buffer (3% normal sheep serum and 0.1% Triton X-100 in PBS; or 5% BSA and 0.5% Triton X-100 in PBS) for 2 h at room temperature. Sections were then incubated in primary antibodies [rat anti-CTIP2 (1:500; Abcam, ab18465), rabbit anti-SATB2 (1:500; Abcam, ab92446), rabbit anti-CUX1 (1:100; Santa Cruz

Development (2021) 148, dev199772. doi:10.1242/dev.199772

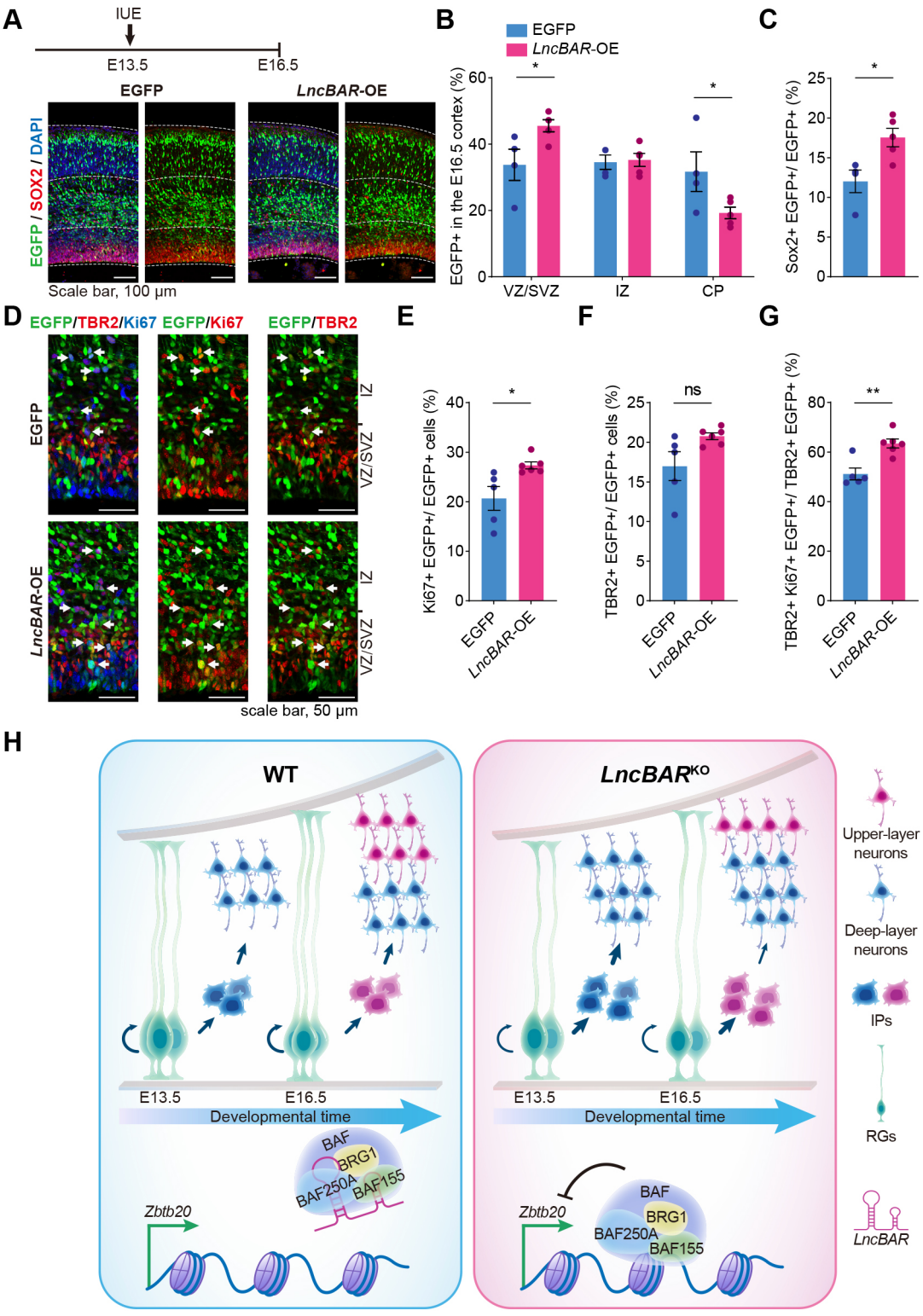


**Fig. 7.** See next page for legend.

Biotechnology, sc-13024), mouse anti-FOXP2 (1:250; Sigma-Aldrich, AMAB91361), rabbit anti-PAX6 (1:500; Millipore, ab2237), rabbit anti-TBR2 (1:500; Abcam, ab23345), rat anti-TBR2 (1:500; Thermo Fisher, 14-4875-82), rabbit anti-SOX2 (1:500; Millipore, ab5603), rabbit anti–Cleaved Caspase-3 (1:100; Cell Signaling Technology, 9664S), rat anti-BrdU (1:500; Abcam, ab6326), mouse-anti-BrdU (1:500; Roche, 11170376001), rabbit anti-Ki67 (1:500; Abcam, ab15580, rabbit anti-doublecortin (1:500; Abcam, ab18723), mouse anti-calretinin (1:250; Santa Cruz, sc-365956), mouse anti-calbindin-D-28K (1:250; Sigma, c9848), rabbit anti-ZBTB20 (1:1000; Sigma, HPA016815) and chicken anti-GFP (1:2000; Abcam, ab13970)] in blocking buffer overnight at 4°C. After three rinses in PBS, sections were incubated in secondary antibodies (Alexa Fluor 488-conjugated anti-mouse, A11029; Alexa Fluor 555-conjugated anti-mouse, A21422; Alexa Fluor 488-conjugated anti-rat, A11006; Alexa

Development (2021) 148, dev199772. doi:10.1242/dev.199772

**Fig. 7. *LncBAR* overexpression (OE) promotes the NPC fate and IP divisions.** (A) Representative images showing E16.5 neocortex transduced with indicated constructs with transduced cells labeled with EGFP. Immunofluorescent images showing expressions of SOX2 in $EGFP^+$ transduced cells. Nuclei were labeled with DAPI (blue). (B) Quantification of localization of $EGFP^+$ transduced cells in E16.5 neocortices. *n*=4 for EGFP, *n*=5 for *LncBAR*-OE. (C) Quantification of $SOX2^+EGFP^+/EGFP^+$ cells. *n*=4 for EGFP, *n*=5 for *LncBAR*-OE. (D) Representative immunofluorescent images showing expression of $Ki67^+/TBR2^+$ in $EGFP^+$ transduced cells at VZ/SVZ-IZ regions. Arrows indicate $EGFP^+/Ki67^+/TBR2^+$ cells. (E-G) Quantification of $Ki67^+EGFP^+/EGFP^+$ (E), $TBR2^+EGFP^+/EGFP^+$ (F) and $TBR2^+Ki67^+EGFP^+/TBR2^+EGFP^+$ (G) cells. *n*=5 for EGFP, *n*=6 for *LncBAR*-OE. (H) Working model. $LncBAR^{KO}$ neocortices contain more deep-layer and fewer upper-layer PNs, but paradoxically more IPs due to compromised proliferative capacity of IPs in mid-late neurogenesis. *LncBAR* functions as a decoy to block the association of the BAF chromatin-remodeling complex with the genomic region of *Zbtb20*. RGs, radial glial cells; IPs, intermediate progenitor cells. Cell counting were performed within frames [830 µm (h)×415 µm (w)] and quantification data are mean±s.e.m. Statistical significance was determined using two-way ANOVA followed by Sidak's multiple comparisons test (B). Statistical significance was determined using Student's two-tailed unpaired *t*-test (C), Student's two-tailed unpaired *t*-test with Welch's correction (E,F) or Mann–Whitney test (G). **P*<0.05; ***P*<0.01; ns, not significant.

Fluor 555-conjugated anti-rat, A21434; Alexa Fluor 647-conjugated anti-rat, A21247; Alexa Fluor 488-conjugated anti-rabbit, A11034; Alexa Fluor 555-conjugated anti-rabbit, A21429; Alexa Fluor 647-conjugated anti-rabbit, A21245; Alexa Fluor 488-conjugated anti-chicken, A11039; Thermo Fisher Scientific; 1:1000) for 1 h at room temperature. Nuclei were labeled by incubation in PBS containing 4′,6-diamidino-2-phenylindole (DAPI) (0.1 µg/ml) (Sigma-Aldrich), and samples were mounted in ProLong Gold Antifade Mountant (Thermo Fisher Scientific).

### Immunohistochemical staining

Frozen brain sections were dried at room temperature, and then pretreated with 0.3% $H_2O_2$ for 15 min to deactivate endogenous peroxidase. Sections were blocked with 3% normal sheep serum with 0.1% Tween 20 at room temperature for 2 h. Sections were then incubated overnight at 4°C with rat anti-BrdU (1:500; Abcam, ab6326) diluted in blocking buffer, followed by addition of the avidin-biotin-peroxidase complex (1:50; VECTASTAIN Elite ABC system, Vector Laboratories). Peroxidase was reacted in 3,3′-diaminobenzidine (5 mg/ml) and 0.075% $H_2O_2$ in Tris-HCl (pH 7.2). Sections were dehydrated in gradient ethanol (75% ethanol, 95% ethanol, 100% ethanol and 100% ethanol, each for 5 min), and cleared twice in xylene for 5 min, then mounted in neutral balsam.

### EdU/BrdU cumulative pulse-labeling experiment

EdU/BrdU cumulative pulse-labeling experiment and calculation methods were adapted from previous works (Harris et al., 2018a,b; Martynoga et al., 2005). Sequential administration of thymidine analogues, 5-ethynyl-2′-deoxyuridine (EdU) (Click-iT Plus EdU Kit, Invitrogen) and 5-bromo-2′-deoxyuridine (BrdU) (Sigma-Aldrich) was applied for cell cycle length assessment. Briefly, pregnant dams (E16.5) were given intraperitoneal injections of EdU (10 mg/kg of body weight), and BrdU (50 mg/kg of body weight) at 0 h and 1.5 h, respectively. After 30 min, embryos were harvested and brains were dissected out. Brains were fixed in 4% PFA at 4°C overnight, dehydrated in 20% sucrose at 4°C overnight and embedded in Tissue-Tek OCT compound (SAKURA). E16.5 brains were cut into 14 µm coronal cryosections. Sections were mounted onto glass slides and then dried for 20 min at 37°C. For antigen retrieval, slides were boiled at 95°C in sodium citrate buffer (10 mM, pH 6.0) for 20 min. Slides were rinsed three times with PBS. EdU detection was carried out using the Click-iT Plus EdU Alexa Fluor 555 Imaging Kit (Invitrogen) according to the manufacturer's protocol. Subsequently, BrdU and TBR2 staining were performed. Sections were incubated in blocking solution (5% w/v BSA and 0.5% v/v Triton-X-100 in PBS) for 2 h at room temperature, then incubated with mouse anti-BrdU (1:500; Roche, 11170376001) and rat anti-TBR2 (1:500; Thermo Fisher, 14-4875-82) antibodies. Immunofluorescence of BrdU and TBR2 were performed as indicated above. Of $TBR2^+$ cells, cells in S-phase were $EdU^+/BrdU^+$ (S-cells), and cells in the leaving fraction were $EdU^+/BrdU^-$ (L-cells). Durations of the S-phase (Ts) and total cell cycle length ($T_C$) were then calculated using the following equations:

$$T_s = T_i \times \frac{S_{cells}}{L_{cells}} = T_i \times \left(\frac{TBR2 + EdU + BrdU + \ cells}{TBR2 + EdU + BrdU - \ cells}\right), \quad (1)$$

$$T_i = 1.5\,\text{h} \quad (2)$$

and

$$\frac{T_s}{T_c} = \frac{S_{fraction}}{Cycling_{fraction}}. \quad (3)$$

The proportion of cells within the population of interest that are in the cell cycle are referred to as the growth fraction (GF). The GF can be determined by examining the proportion of $TBR2^+$ cells that can be labeled with the cell-cycle marker Ki67, given by the formula:

$$GF = \frac{TBR2 + Ki67 + cells}{TBR2 + cells}. \quad (4)$$

We then used the following formula to determine Tc:

$$T_C = T_S \times \frac{Cycling_{fraction}}{S_{fraction}} = T_S \times \frac{TBR2 + cells \times GF}{TBR2 + BrdU +}. \quad (5)$$

### Biotin-labeled RNA pull-down

RNA pull-down was performed as described previously (Li et al., 2020; Tsai et al., 2010). Biotinylated RNAs were transcribed using the Biotin-RNA Labeling Mix (Roche) and HiScribe T7 High Yield RNA Synthesis Kit (NEB) according to the manufacturer's protocol. About 3 µg of biotinylated RNA supplied with RNA structure buffer [10 mmol/l Tris (pH 7), 0.1 mol/l KCl, 10 mmol/l $MgCl_2$) was heated at 90°C for 2 min, chilled on ice for 2 min and then shifted to room temperature for 20 min. Approximately 4-6×$10^7$ primary cells from E14.5 mouse cortices were used for each RNA pull-down experiment. Cells were resuspended in 2 ml PBS, 2 ml nuclear isolation buffer [1.28 mol/l sucrose; 40 mmol/l Tris-HCl (pH 7.5); 20 mmol/l $MgCl_2$; 4% Triton X-100] and 6 ml water for 20 min on ice. Nuclei were pelleted by centrifugation at 2500 ***g*** for 15 min and resuspended in 1 ml RIP buffer [150 mmol/l KCl, 25 mmol/l Tris (pH 7.4), 0.5 mmol/l DTT, 0.5% NP-40, 1 mmol/l PMSF and protease inhibitor cocktail (Biotool)]. Resuspended nuclei were sonicated on ice at 30% power output for 3 min (0.5 s on, 0.5 s off). Nuclear extracts were collected by centrifugation at 15,294 ***g*** for 10 min, and were pre-cleared by 40 µl streptavidin agarose (Thermo Fisher) and 20 µg/ml yeast tRNA for 30 min at 4°C with rotation. Pre-cleared lysates were mixed with 3 µg folded biotinylated RNA probes at 4°C overnight, followed by adding 60 µl washed streptavidin agarose beads to each binding reaction and incubating at room temperature for 1.5 h. After incubation, streptavidin agarose beads were washed for 4×10 min by RIP buffer (containing 0.5% sodium deoxycholate) at 4°C. Proteins bound to RNA were eluted in 1× SDS sample buffer by boiling at 100°C for 10 min, and then subjected to SDS-PAGE and visualized by silver staining. Finally, proteins were identified by mass spectrometry. The primers used are listed in Table S3.

### UV-crosslinking RNA immunoprecipitation

The procedure of RNA immunoprecipitation was adapted from a previous publication (Ule et al., 2005). Neuro-2a cells in 100 mm plates were washed twice with 5 ml of ice-cold PBS, and placed in HL-2000 Hybrilinker with the cover off. Cells were irradiated at 200 mJ/$cm^2$ at 254 nm on ice for 1 min. Cells were harvested in PBS and collected by centrifugation at 1699 ***g*** at 4°C for 5 min. Cells were homogenized in 1 ml buffer A [1× PBS, 0.1% SDS, 0.5% deoxycholate, 0.5% NP-40, 1 mmol/l PMSF, 2 mmol/l RVC, protease inhibitor cocktail (Biotool)], followed by sonication with a 25% power output for 5 min (0.5 s on, 0.5 s off) on ice. For each tube, 20 µl DNase I (Thermo Fisher) was added followed by incubation at 37°C for

Development (2021) 148, dev199772. doi:10.1242/dev.199772

5-10 min. After centrifuging at 15,294 ***g*** at 4°C for 10 min, the supernatant was precleared with 30 µl protein G agarose beads and 20 µg/ml yeast tRNA at 4°C for 30 min. Then the pre-cleared lysate was incubated with 50 µl protein G agarose beads pre-coated with 3 µg control IgG antibody (ABclonal, AC005) or anti-BRG1 antibody (Proteintech, 21634-1-AP) at 4°C for 4 h. The agarose beads were washed for 4×10 min with buffer A (1× PBS, 0.1% SDS, 0.5% deoxycholate and 0.5% NP-40), for 2×10 min in Buffer B (5× PBS, 0.1% SDS, 0.5% deoxycholate and 0.5% NP-40) and for 2×10 min in Buffer C [50 mM Tris–HCl (pH 7.4), 10 mM $MgCl_2$, 0.5% NP-40]. 5 µl of 20 mg/ml proteinase K were then added to beads and incubated at 37°C for 30 min. RNAs were extracted with RNAiso Plus solution (Takara). Reverse transcription was performed with PrimerScript Reverse Transcriptase (Takara) using random primers followed by qRT-PCR analysis. The primers used are listed in Table S3.

### Western blot analysis

The brain tissue or cultured cells were collected, homogenized and centrifuged according to standard protocols. Protein samples were loaded, along with a molecular weight marker (Thermo Fisher Scientific), onto 8 or 12% SDS-polyacrylamide gel electrophoresis gels. Immunoblot analysis was carried out used the following antibodies: rabbit anti-H3 (1:10,000; ABclonal, A2348), rabbit anti-actin (1:100,000; ABclonal, AC026), rabbit anti-BRG1 (1:1000; Proteintech, 21634-1-AP), rabbit anti-SMARCA4 (1:1000, CST, 49360), rabbit anti-BAF170 (1:1000; ABclonal, A1967), rabbit anti-BAF155 (1:1000; ABclonal, A6128), rabbit anti-BAF250a (1:1000; ABclonal, A16648), mouse anti-BAF250a (1:1000; Santa Cruz, sc-32761), rabbit anti-BAF57 (1:1000; ABclonal, A13353) and rabbit anti-ZBTB20 (1:1000; Sigma, HPA016815).

### *In utero* electroporation (IUE) of developing neocortices

*In utero* microinjection and electroporation were performed at E13.5 as previously described (Li et al., 2017). Pregnant CD-1 (for *LncBAR*-OE) or C57BL/6 (for ZBTB20 gain-of-function) mice with E13.5 embryos were anesthetized by injection of pentobarbital sodium (70 mg/kg), and the uteri were exposed through a 2 cm midline abdominal incision. Embryos were carefully pulled out using ring forceps through the incision and placed on sterile gauze wet with 0.9% sodium chloride. Plasmid DNA (prepared using Endo Free plasmid purification kit, Tiangen) mixed with 0.05% Fast Green (Sigma) was injected through the uterine wall into the telencephalic vesicle using pulled borosilicate needles (WPI). For gain-of-function experiments, pCIG (1 µg/µl) was mixed with pCAGGS-ZBTB20, with pCAGGGS-ZBTB20-ΔZnf or with pCAGGS-*LncBAR* (3 µg/µl each). Control mice were injected with pCIG (1 µg/µl). Five electric pulses (36 V, 50 ms duration at 1 s intervals) were generated using CUY21VIVO-SQ (BEX) and delivered across the head of embryos using 5 mm forceps-like electrodes (BEX). The uteri were then carefully put back into the abdominal cavity, and both peritoneum and abdominal skin were sewed with surgical sutures. The whole procedure was completed within 30 min. Mice were warmed on a heating pad until they regained consciousness and were treated with analgesia (ibuprofen in drinking water) until sacrifice at E16.5.

### RNA-seq and data analysis

Cultured neurospheres were collected and total RNAs were extracted. The integrity of RNAs was analyzed using Agilent Bioanalyzer 2100. RNA-seq were performed in Novogene (Beijing, China). RNA-seq library construction and data processing were performed as described previously (Xu et al., 2021). RNA-seq libraries were constructed using the NEBNext Ultra II RNA Library Prep Kit for Illumina (New England Biolabs, no. E7775), and were sequenced by the Illumina NovaSeq 6000 platform with pair-end reads of 150 bp. The sequencing depth was 60 million reads per library. All RNA-seq raw fastq data were cleaned by removing the adaptor sequence. Cleaned RNA-seq reads were processed by mapping to the mm10 reference mouse genome using TopHat (version 2.1.1; http://ccb.jhu.edu/software/tophat/index.shtml) with default settings. The gene expression level was calculated by Cufflinks (version 2.2.1; http://cole-trapnell-lab.github.io/cufflinks) and normalized by fragments per kilobase of bin per million mapped reads. Differentially expressed genes are defined as ones with $P<0.05$. To determine significantly enriched Gene Ontology terms ($P$ value<0.05), Database for Annotation, Visualization and Integrated Discovery (DAVID, version 6.8) was used. Differentially expressed genes comparing E12.5 WT and $LncBAR^{KO}$ neurospheres are listed in Table S2.

### ChIP assay

ChIP-seq was performed as described previously (Xu et al., 2021). For each experiment, single-cell suspensions from E12.5 neurosphere were collected. Cells were cross-linked with 1% formaldehyde for 10 min at room temperature and then quenched with 0.125 M glycine for 5 min. Cross-linked samples were then rinsed in PBS twice, and harvested in ice-cold IP buffer [100 mM NaCl, 50 mM tris-HCl (pH 8.1), 5 mM EDTA (pH 8.0), 0.02% $NaN_3$, 0.5% SDS, 1× protease inhibitor cocktail and 1 mM phenylmethylsulfonyl fluoride], followed by sonication in a Bioruptor Pico (Diagenode) at a setting of '30 s on, 30 s off, 30 cycles' at 4°C. Samples were sonicated to an average length of 200-500 bp, and 20 µl were taken for checking the efficiency of sonication. 30 µl lysate (3%) was kept to quantify DNA before immunoprecipitation (input). Immunoprecipitation was further performed with sheared chromatin and 3 µg anti-BRG1 antibody (Proteintech, 21634-1-AP) overnight at 4°C with rotation. The next day, immunocomplexes were incubated with 50 µl Protein G sepharose beads for 4 h at 4°C, followed by three washes with wash buffer I [20 mM Tris-HCl (pH 8.0), 150 mM NaCl, 2 mM EDTA, 1% Triton X-100 and 0.1% SDS] and one wash with wash buffer II [20 mM Tris-HCl (pH 8.0), 500 mM NaCl, 2 mM EDTA, 1% Triton X-100 and 0.1% SDS]. Protein-DNA complexes were de-crosslinked in 120 µl de-crossed buffer (TE buffer) and shaken at 65°C for 3 h. DNA extraction, precipitation and resuspension were performed using DNA purification kit (Qiagen).

### ENCODE data processing

In Fig. S1, we showed results of ChIP-seq signals for H3K36me3 in developing forebrains at E10.5, E12.5, E16.5 and P0; RNA-seq signals in neocortex at E12.5, E16.5 and P0; and *LncBAR* expression in different tissues of 8-week-old mice. Data were downloaded from the Mouse ENCODE project (Davis et al., 2018) with the following identifiers: ENCSR558NWQ, ENCSR345DDI, ENCSR352AWJ, ENCSR069TDC (H3K36me3 ChIP-seq); ENCSR647QBV, ENCSR080EVZ, ENCSR362AIZ (RNA-seq); ENCSR000BZS, ENCSR000BZR, ENCSR000BZM, ENCSR000BYY, ENCSR000BYZ, ENCSR000BYQ, ENCSR000BYR, ENCSR000BYX, ENCSR000BYT, ENCSR000BYS, ENCSR000BZA, ENCSR000BZD, ENCSR000BZB, ENCSR000BZC, ENCSR000BZP, ENCSR000BYU, ENCSR000BZE, ENCSR000BZF, ENCSR000BYW, ENCSR000BYV and ENCSR000BZQ (8-week-old mice) (https://www.encodeproject.org/).

### Plasmid construction

Full-length mouse *LncBAR* was amplified from cDNAs of E18.5 mouse cortex and then cloned into pCAGGS. Full-length *Zbtb20* and *Zbtb20* with deletion of the zinc-finger domain (*Zbtb20-ΔZnf*) were amplified from cDNAs of P0 mouse hippocampus, and then cloned into pCAGGS. The primers used are listed in Table S3.

### Cell transfection

The day before transfection, Neuro-2a cells were seeded in a 10 cm dish for 16 h. In Polyethyleneimine (PEI) transfection system, 12 µg of pCAGGS-*LncBAR* was diluted into 500 µl of Opti-MEM medium. PEI was added to the plasmids mix with a plasmid:PEI ratio of 1:2, and the mix was incubated for 20-30 min at room temperature. The plasmids:PEI mixture was then added dropwise to each well (Xu et al., 2021). Two days after transfection, cells were harvested and total RNAs were extracted for northern blotting.

### Image acquisition

Confocal images were acquired using Zeiss LSM 880 with Airyscan with a 20× or 40× objective at 1024×1024 pixel resolution. Brightness and contrast were adjusted, and images were merged with Adobe Photoshop CC (version 20.0.0). Bright-field images were taken using Leica Aperio VERSA 8 and

Aperio ImageScope software (Leica). The total number of marker-positive cells in the brain sections was quantified by counting positive cells in sections with anatomically matched positions in experimental groups. For whole-mount embryos or brains, images were collected using a Nikon 80i microscope equipped with Nikon DS-FI1C-U3 camera system. Measurements of the thickness of cortex were made using Adobe Photoshop CC (version 20.0.0). The length and area of OB and neocortical hemispheres were measured using ImageJ. Results were obtained from at least three mouse brains of each genotype.

### Quantification and statistical analysis

No statistical method was used to predetermine sample size. The experiments were not randomized and the investigators were not blinded to allocation during experiments. Experiments performed on genotyping were blinded by post-experimental determination of genotypes. Results are presented as the mean±s.e.m. or ±s.d. The statistical significance of a single comparison between two groups was performed using Student's two-tailed unpaired *t*-test with Welch's correction when required (non-equal variances) or the Mann–Whitney nonparametric test when data did not fit a normal distribution (assessed using the Shapiro–Wilk normality test). The proportion of cortical layers and distribution of $BrdU^+$ cells was analyzed using two-way ANOVA followed by Sidak's multiple comparisons test, the normality of data was assessed using the Shapiro–Wilk normality test. For the ZBTB20 rescue experiment, the distribution of $EGFP^+$ cells was analyzed using two-way ANOVA followed by Tukey's multiple comparisons test. The normality of data was assessed using the Shapiro–Wilk normality test. The quantifications of double- or triple-labeled cells were analyzed using one-way ANOVA followed by Tukey's post-hoc test after checking that our data fit to a normal distribution (assessed by Shapiro–Wilk normality test) and the variance of the difference was equal (determined by Brown-Forsythe's test). For the *LncBAR* overexpression experiments, the distribution of $EGFP^+$ cells were analyzed using two-way ANOVA followed by Sidak's multiple comparisons test, and the normality of data was assessed by Shapiro–Wilk normality test. Statistical plots and tests were conducted using GraphPad Prism (version 8.0.2). The value of *n* for each graph was stated in the figure legends. Significant difference is indicated by $P<0.05$ ($*P<0.05$, $**P<0.01$, $***P<0.001$ and $****P<0.0001$). For details of statistical methods, see Table S4.

#### Acknowledgements

We thank all Zhou members for their critical reading of the manuscript.

#### Competing interests

The authors declare no competing or financial interests.

#### Author contributions

Conceptualization: A.W., Y.L., Y. Zhou; Software: C.Z.; Formal analysis: K.T.; Investigation: A.W., J.W., K.T., D.H., H.Y., S.L., B.Z., Y. Zheng, L.X., X.H., K.W., Q.-F.W., X.W.; Data curation: A.W., J.W., K.T.; Writing - original draft: A.W., J.W., K.T., Y.L., Y. Zhou; Visualization: A.W.; Supervision: T.Z., Y. Zhou; Project administration: Y. Zhou; Funding acquisition: Y. Zhou.

#### Funding

This work was supported by grants from the National Key R&D Program of China (2018YFA0800700), the National Natural Science Foundation of China (31970770 and 31970676), the Medical Science Advancement Program (Basic Medical Sciences) of Wuhan University (TFJC2018005) and the State Key Laboratory Special Fund (2060204).

#### Data availability

BRG1 ChIP-Seq and RNA-Seq for E12.5 wild-type and $LncBAR^{KO}$ neurospheres have been deposited in GEO under accession number GSE169167.

#### Peer review history

The peer review history is available online at https://journals.biologists.com/dev/article-lookup/doi/10.1242/dev.199772.

#### References

**Arai, Y., Pulvers, J. N., Haffner, C., Schilling, B., Nüsslein, I., Calegari, F. and Huttner, W. B.** (2011). Neural stem and progenitor cells shorten S-phase on commitment to neuron production. *Nat. Commun.* **2**, 154. doi:10.1038/ncomms1155

**Braun, S. M. G., Petrova, R., Tang, J., Krokhotin, A., Miller, E. L., Tang, Y., Panagiotakos, G. and Crabtree, G. R.** (2021). BAF subunit switching regulates chromatin accessibility to control cell cycle exit in the developing mammalian cortex. *Genes Dev.* **35**, 335-353. doi:10.1101/gad.342345.120

**Cabianca, D. S., Casa, V., Bodega, B., Xynos, A., Ginelli, E., Tanaka, Y. and Gabellini, D.** (2012). A long ncRNA links copy number variation to a polycomb/trithorax epigenetic switch in FSHD muscular dystrophy. *Cell* **149**, 819-831. doi:10.1016/j.cell.2012.03.035

**Cajigas, I., Leib, D. E., Cochrane, J., Luo, H., Swyter, K. R., Chen, S., Clark, B. S., Thompson, J., Yates, J. R., III, Kingston, R. E. et al.** (2015). Evf2 lncRNA/BRG1/DLX1 interactions reveal RNA-dependent inhibition of chromatin remodeling. *Development* **142**, 2641-2652. doi:10.1242/dev.126318

**Calegari, F., Haubensak, W., Haffner, C. and Huttner, W. B.** (2005). Selective lengthening of the cell cycle in the neurogenic subpopulation of neural progenitor cells during mouse brain development. *J. Neurosci.* **25**, 6533-6538. doi:10.1523/JNEUROSCI.0778-05.2005

**Caviness, V. S., Jr and Rakic, P.** (1978). Mechanisms of cortical development: a view from mutations in mice. *Annu. Rev. Neurosci.* **1**, 297-326. doi:10.1146/annurev.ne.01.030178.001501

**Chalei, V., Sansom, S. N., Kong, L., Lee, S., Montiel, J. F., Vance, K. W. and Ponting, C. P.** (2014). The long non-coding RNA Dali is an epigenetic regulator of neural differentiation. *eLife* **3**, e04530. doi:10.7554/eLife.04530

**Choi, H. M. T., Schwarzkopf, M., Fornace, M. E., Acharya, A., Artavanis, G., Stegmaier, J., Cunha, A. and Pierce, N. A.** (2018). Third-generation in situ hybridization chain reaction: multiplexed, quantitative, sensitive, versatile, robust. *Development* **145**, dev.165753.

**Davis, C. A., Hitz, B. C., Sloan, C. A., Chan, E. T., Davidson, J. M., Gabdank, I., Hilton, J. A., Jain, K., Baymuradov, U. K., Narayanan, A. K. et al.** (2018). The Encyclopedia of DNA elements (ENCODE): data portal update. *Nucleic Acids Res.* **46**, D794-D801. doi:10.1093/nar/gkx1081

**Dehay, C. and Kennedy, H.** (2007). Cell-cycle control and cortical development. *Nat. Rev. Neurosci.* **8**, 438-450. doi:10.1038/nrn2097

**Doeppner, T. R., Herz, J., Bähr, M., Tonchev, A. B. and Stoykova, A.** (2019). Zbtb20 regulates developmental neurogenesis in the olfactory bulb and gliogenesis after adult brain injury. *Mol. Neurobiol.* **56**, 567-582. doi:10.1007/s12035-018-1104-y

**Dubreuil, V., Hirsch, M. R., Pattyn, A., Brunet, J. F. and Goridis, C.** (2000). The Phox2b transcription factor coordinately regulates neuronal cell cycle exit and identity. *Development* **127**, 5191-5201. doi:10.1242/dev.127.23.5191

**Dyer, M. A. and Cepko, C. L.** (2001). p27Kip1 and p57Kip2 regulate proliferation in distinct retinal progenitor cell populations. *J. Neurosci.* **21**, 4259-4271. doi:10.1523/JNEUROSCI.21-12-04259.2001

**Florio, M. and Huttner, W. B.** (2014). Neural progenitors, neurogenesis and the evolution of the neocortex. *Development* **141**, 2182-2194. doi:10.1242/dev.090571

**Franco, S. J. and Müller, U.** (2013). Shaping our minds: stem and progenitor cell diversity in the mammalian neocortex. *Neuron* **77**, 19-34. doi:10.1016/j.neuron.2012.12.022

**Fuentealba, L. C., Rompani, S. B., Parraguez, J. I., Obernier, K., Romero, R., Cepko, C. L. and Alvarez-Buylla, A.** (2015). Embryonic origin of postnatal neural stem cells. *Cell* **161**, 1644-1655. doi:10.1016/j.cell.2015.05.041

**Furutachi, S., Miya, H., Watanabe, T., Kawai, H., Yamasaki, N., Harada, Y., Imayoshi, I., Nelson, M., Nakayama, K. I., Hirabayashi, Y. et al.** (2015). Slowly dividing neural progenitors are an embryonic origin of adult neural stem cells. *Nat. Neurosci.* **18**, 657-665. doi:10.1038/nn.3989

**Garcia, M. T., Chang, Y. J., Arai, Y. and Huttner, W. B.** (2016). S-phase duration is the main target of cell cycle regulation in neural progenitors of developing ferret neocortex. *J. Comp. Neurol.* **524**, 456-470. doi:10.1002/cne.23801

**Geng, A., Qiu, R., Murai, K., Liu, J., Wu, X., Zhang, H., Farhoodi, H., Duong, N., Jiang, M., Yee, J.-K. et al.** (2018). KIF20A/MKLP2 regulates the division modes of neural progenitor cells during cortical development. *Nat. Commun.* **9**, 2707. doi:10.1038/s41467-018-05152-1

**Greig, L. C., Woodworth, M. B., Galazo, M. J., Padmanabhan, H. and Macklis, J. D.** (2013). Molecular logic of neocortical projection neuron specification, development and diversity. *Nat. Rev. Neurosci.* **14**, 755-769. doi:10.1038/nrn3586

**Han, P., Li, W., Lin, C.-H., Yang, J., Shang, C., Nuernberg, S. T., Jin, K. K., Xu, W., Lin, C.-Y., Lin, C.-J. et al.** (2014). A long noncoding RNA protects the heart from pathological hypertrophy. *Nature* **514**, 102-106. doi:10.1038/nature13596

**Harris, L., Zalucki, O. and Piper, M.** (2018a). BrdU/EdU dual labeling to determine the cell-cycle dynamics of defined cellular subpopulations. *J. Mol. Histol.* **49**, 229-234. doi:10.1007/s10735-018-9761-8

**Harris, L., Zalucki, O. and Piper, M.** (2018b). Correction to: BrdU/EdU dual labeling to determine the cell-cycle dynamics of defined cellular subpopulations. *J. Mol. Histol.* **49**, 447. doi:10.1007/s10735-018-9783-2

**Haubensak, W., Attardo, A., Denk, W. and Huttner, W. B.** (2004). Neurons arise in the basal neuroepithelium of the early mammalian telencephalon: A major site of

neurogenesis. *Proc. Natl Acad Sci USA* **101**, 3196-3201. doi:10.1073/pnas.0308600100

**Hutton, S. R. and Pevny, L. H.** (2011). SOX2 expression levels distinguish between neural progenitor populations of the developing dorsal telencephalon. *Dev. Biol.* **352**, 40-47. doi:10.1016/j.ydbio.2011.01.015

**Jones, K. A., Luo, Y., Dukes-Rimsky, L., Srivastava, D. P., Koul-Tewari, R., Russell, T. A., Shapiro, L. P., Srivastava, A. K. and Penzes, P.** (2018). Neurodevelopmental disorder-associated ZBTB20 gene variants affect dendritic and synaptic structure. *Plos One* **13**, e0203760. doi:10.1371/journal.pone.0203760

**Kowalczyk, T., Pontious, A., Englund, C., Daza, R. A. M., Bedogni, F., Hodge, R., Attardo, A., Bell, C., Huttner, W. B. and Hevner, R. F.** (2009). Intermediate Neuronal Progenitors (Basal Progenitors) Produce Pyramidal-Projection Neurons for All Layers of Cerebral Cortex. *Cereb. Cortex* **19**, 2439-2450. doi:10.1093/cercor/bhn260

**Kriegstein, A. and Alvarez-Buylla, A.** (2009). The glial nature of embryonic and adult neural stem cells. *Annu. Rev. Neurosci.* **32**, 149-184. doi:10.1146/annurev.neuro.051508.135600

**Kriegstein, A., Noctor, S. and Martínez-Cerdeño, V.** (2006). Patterns of neural stem and progenitor cell division may underlie evolutionary cortical expansion. *Nat. Rev. Neurosci.* **7**, 883-890. doi:10.1038/nrn2008

**Lange, C. and Calegari, F.** (2010). Cdks and cyclins link G1 length and differentiation of embryonic, neural and hematopoietic stem cells. *Cell Cycle* **9**, 1893-1900. doi:10.4161/cc.9.10.11598

**Lange, C., Huttner, W. B. and Calegari, F.** (2009). Cdk4/CyclinD1 Overexpression in Neural Stem Cells Shortens G1, Delays Neurogenesis, and Promotes the Generation and Expansion of Basal Progenitors. *Cell Stem Cell* **5**, 320-331. doi:10.1016/j.stem.2009.05.026

**Lessard, J., Wu, J. I., Ranish, J. A., Wan, M., Winslow, M. M., Staahl, B. T., Wu, H., Aebersold, R., Graef, I. A. and Crabtree, G. R.** (2007). An essential switch in subunit composition of a chromatin remodeling complex during neural development. *Neuron* **55**, 201-215. doi:10.1016/j.neuron.2007.06.019

**Li, Y. M., Wang, W., Wang, F. Y., Wu, Q. S., Li, W., Zhong, X. L., Tian, K., Zeng, T., Gao, L., Liu, Y. et al.** (2017). Paired related homeobox 1 transactivates dopamine D2 receptor to maintain propagation and tumorigenicity of glioma-initiating cells. *J. Mol. Cell Biol.* **9**, 302-314. doi:10.1093/jmcb/mjx017

**Li, W., Shen, W. H., Zhang, B., Tian, K., Li, Y. M., Mu, L. L., Luo, Z. Y., Zhong, X. L., Wu, X. D., Liu, Y. et al.** (2020). Long non-coding RNA LncKdm2b regulates cortical neuronal differentiation by cis-activating Kdm2b. *Protein Cell* **11**, 161-186. doi:10.1007/s13238-019-0650-z

**Lim, S. and Kaldis, P.** (2012). Loss of Cdk2 and Cdk4 induces a switch from proliferation to differentiation in neural stem cells. *Stem Cells* **30**, 1509-1520. doi:10.1002/stem.1114

**Lino Cardenas, C. L., Kessinger, C. W., Cheng, Y., MacDonald, C., MacGillivray, T., Ghoshhajra, B., Huleihel, L., Nuri, S., Yeri, A. S., Jaffer, F. A. et al.** (2018). An HDAC9-MALAT1-BRG1 complex mediates smooth muscle dysfunction in thoracic aortic aneurysm. *Nat. Commun.* **9**, 1009. doi:10.1038/s41467-018-03394-7

**Lui, J. H., Hansen, D. V. and Kriegstein, A. R.** (2011). Development and evolution of the human neocortex. *Cell* **146**, 18-36. doi:10.1016/j.cell.2011.06.030

**Luo, Z. Y., Mu, L. L., Zheng, Y., Shen, W. C., Li, J. L., Xu, L. C., Zhong, B., Liu, Y. and Zhou, Y.** (2020). NUMB enhances Notch signaling by repressing ubiquitination of NOTCH1 intracellular domain. *J. Mol. Cell Biol.* **12**, 345-358. doi:10.1093/jmcb/mjz088

**Martinez-Cerdeno, V., Noctor, S. C. and Kriegstein, A. R.** (2006). The role of intermediate progenitor cells in the evolutionary expansion of the cerebral cortex. *Cereb. Cortex* **16**, I152-I161. doi:10.1093/cercor/bhk017

**Martynoga, B., Morrison, H., Price, D. J. and Mason, J. O.** (2005). Foxg1 is required for specification of ventral telencephalon and region-specific regulation of dorsal telencephalic precursor proliferation and apoptosis. *Dev. Biol.* **283**, 113-127. doi:10.1016/j.ydbio.2005.04.005

**Mihalas, A. B., Elsen, G. E., Bedogni, F., Daza, R. A. M., Ramos-Laguna, K. A., Arnold, S. J. and Hevner, R. F.** (2016). Intermediate progenitor cohorts differentially generate cortical layers and require Tbr2 for timely acquisition of neuronal subtype identity. *Cell Rep.* **16**, 92-105. doi:10.1016/j.celrep.2016.05.072

**Molyneaux, B. J., Arlotta, P., Menezes, J. R. L. and Macklis, J. D.** (2007). Neuronal subtype specification in the cerebral cortex. *Nat. Rev. Neurosci.* **8**, 427-437. doi:10.1038/nrn2151

**Mu, W., Li, S., Xu, J., Guo, X., Wu, H., Chen, Z., Qiao, L., Helfer, G., Lu, F., Liu, C. et al.** (2021). Hypothalamic Rax(+) tanycytes contribute to tissue repair and tumorigenesis upon oncogene activation in mice. *Nat. Commun.* **12**, 2288. doi:10.1038/s41467-021-22640-z

**Narayanan, R. and Tuoc, T. C.** (2014). Roles of chromatin remodeling BAF complex in neural differentiation and reprogramming. *Cell Tissue Res.* **356**, 575-584. doi:10.1007/s00441-013-1791-7

**Narayanan, R., Pirouz, M., Kerimoglu, C., Pham, L., Wagener, R. J., Kiszka, K. A., Rosenbusch, J., Seong, R. H., Kessel, M., Fischer, A. et al.** (2015). Loss of BAF (mSWI/SNF) complexes causes global transcriptional and chromatin state changes in forebrain development. *Cell Rep* **13**, 1842-1854. doi:10.1016/j.celrep.2015.10.046

**Narayanan, R., Pham, L., Kerimoglu, C., Watanabe, T., Castro Hernandez, R., Sokpor, G., Ulmke, P. A., Kiszka, K. A., Tonchev, A. B., Rosenbusch, J. et al.** (2018). Chromatin remodeling BAF155 subunit regulates the genesis of basal progenitors in developing cortex. *iScience* **4**, 109-126. doi:10.1016/j.isci.2018.05.014

**Nguyen, H., Sokpor, G., Pham, L., Rosenbusch, J., Stoykova, A., Staiger, J. F. and Tuoc, T.** (2016). Epigenetic regulation by BAF (mSWI/SNF) chromatin remodeling complexes is indispensable for embryonic development. *Cell cycle* **15**, 1317-1324. doi:10.1080/15384101.2016.1160984

**Nguyen, H., Kerimoglu, C., Pirouz, M., Pham, L., Kiszka, K. A., Sokpor, G., Sakib, M. S., Rosenbusch, J., Teichmann, U., Seong, R. H. et al.** (2018). Epigenetic regulation by BAF complexes limits neural stem cell proliferation by suppressing Wnt signaling in late embryonic development. *Stem Cell Rep.* **10**, 1734-1750. doi:10.1016/j.stemcr.2018.04.014

**Nielsen, J. V., Nielsen, F. H., Ismail, R., Noraberg, J. and Jensen, N. A.** (2007). Hippocampus-like corticoneurogenesis induced by two isoforms of the BTB-zinc finger gene Zbtb20 in mice. *Development* **134**, 1133-1140. doi:10.1242/dev.000265

**Nielsen, J. V., Blom, J. B., Noraberg, J. and Jensen, N. A.** (2010). Zbtb20-induced CA1 pyramidal neuron development and area enlargement in the cerebral midline cortex of mice. *Cereb. Cortex* **20**, 1904-1914. doi:10.1093/cercor/bhp261

**Noctor, S. C., Martínez-Cerdeño, V., Ivic, L. and Kriegstein, A. R.** (2004). Cortical neurons arise in symmetric and asymmetric division zones and migrate through specific phases. *Nat. Neurosci.* **7**, 136-144. doi:10.1038/nn1172

**Oberst, P., Fièvre, S., Baumann, N., Concetti, C., Bartolini, G. and Jabaudon, D.** (2019). Temporal plasticity of apical progenitors in the developing mouse neocortex. *Nature* **573**, 370-374. doi:10.1038/s41586-019-1515-6

**Okazaki, Y., Furuno, M., Kasukawa, T., Adachi, J., Bono, H., Kondo, S., Nikaido, I., Osato, N., Saito, R., Suzuki, H. et al.** (2002). Analysis of the mouse transcriptome based on functional annotation of 60,770 full-length cDNAs. *Nature* **420**, 563-573. doi:10.1038/nature01266

**Orford, K. W. and Scadden, D. T.** (2008). Deconstructing stem cell self-renewal: genetic insights into cell-cycle regulation. *Nat. Rev. Genet.* **9**, 115-128. doi:10.1038/nrg2269

**Qian, X. M., Shen, Q., Goderie, S. K., He, W. L., Capela, A., Davis, A. A. and Temple, S.** (2000). Timing of CNS cell generation: a programmed sequence of neuron and glial cell production from isolated murine cortical stem cells. *Neuron* **28**, 69-80. doi:10.1016/S0896-6273(00)00086-6

**Ramos, A. D., Andersen, R. E., Liu, S. J., Nowakowski, T. J., Hong, S. J., Gertz, C. C., Salinas, R. D., Zarabi, H., Kriegstein, A. R. and Lim, D. A.** (2015). The long noncoding RNA Pnky regulates neuronal differentiation of embryonic and postnatal neural stem cells. *Cell Stem Cell* **16**, 439-447. doi:10.1016/j.stem.2015.02.007

**Ritchie, K., Seah, C., Moulin, J., Isaac, C., Dick, F. and Bérubé, N. G.** (2008). Loss of ATRX leads to chromosome cohesion and congression defects. *J. Cell Biol.* **180**, 315-324. doi:10.1083/jcb.200706083

**Ritchie, K., Watson, L. A., Davidson, B., Jiang, Y. and Bérubé, N. G.** (2014). ATRX is required for maintenance of the neuroprogenitor cell pool in the embryonic mouse brain. *Biol. Open* **3**, 1158-1163. doi:10.1242/bio.20148730

**Salomoni, P. and Calegari, F.** (2010). Cell cycle control of mammalian neural stem cells: putting a speed limit on G1. *Trends Cell Biol.* **20**, 233-243. doi:10.1016/j.tcb.2010.01.006

**Seo, S., Herr, A., Lim, J. W., Richardson, G. A., Richardson, H. and Kroll, K. L.** (2005). Geminin regulates neuronal differentiation by antagonizing Brg1 activity. *Genes Dev.* **19**, 1723-1734. doi:10.1101/gad.1319105

**Sessa, A., Mao, C.-A., Hadjantonakis, A.-K., Klein, W. H. and Broccoli, V.** (2008). Tbr2 directs conversion of radial Glia into basal precursors and guides neuronal amplification by indirect neurogenesis in the developing neocortex. *Neuron* 60, 56-69. doi:10.1016/j.neuron.2008.09.028

**Singh, A. M. and Dalton, S.** (2009). The cell cycle and Myc intersect with mechanisms that regulate pluripotency and reprogramming. *Cell Stem Cell* **5**, 141-149. doi:10.1016/j.stem.2009.07.003

**Sokpor, G., Xie, Y. B., Rosenbusch, J. and Tuoc, T.** (2017). Chromatin remodeling BAF (SWI/SNF) complexes in neural development and disorders. *Front. Mol. Neurosci.* **10**, 243. doi:10.3389/fnmol.2017.00243

**Sokpor, G., Castro-Hernandez, R., Rosenbusch, J., Staiger, J. F. and Tuoc, T.** (2018). ATP-dependent chromatin remodeling during cortical neurogenesis. *Front. Neurosci.* **12**, 226. doi:10.3389/fnins.2018.00226

**Staahl, B. T., Tang, J., Wu, W., Sun, A., Gitler, A. D., Yoo, A. S. and Crabtree, G. R.** (2013). Kinetic analysis of npBAF to nBAF switching reveals exchange of SS18 with CREST and integration with neural developmental pathways. *J. Neurosci.* **33**, 10348-10361. doi:10.1523/JNEUROSCI.1258-13.2013

**Tian, K., Wang, A. D., Wang, J. B., Li, W., Shen, W. C., Li, Y. M., Luo, Z. Y., Liu, Y. and Zhou, Y.** (2021). Transcriptome analysis identifies SenZfp536, a sense LncRNA that suppresses self-renewal of cortical neural progenitors. *Neurosci. Bull.* **37**, 183-200. doi:10.1007/s12264-020-00607-2

**Tonchev, A. B., Tuoc, T. C., Rosenthal, E. H., Studer, M. and Stoykova, A.** (2016). Zbtb20 modulates the sequential generation of neuronal layers in developing cortex. *Mol. Brain* **9**, 65. doi:10.1186/s13041-016-0242-2

**Tsai, M.-C., Manor, O., Wan, Y., Mosammaparast, N., Wang, J. K., Lan, F., Shi, Y., Segal, E. and Chang, H. Y.** (2010). Long noncoding RNA as modular scaffold of histone modification complexes. *Science* **329**, 689-693. doi:10.1126/science.1192002

**Tuoc, T. C., Boretius, S., Sansom, S. N., Pitulescu, M. E., Frahm, J., Livesey, F. J. and Stoykova, A.** (2013). Chromatin regulation by BAF170 controls cerebral cortical size and thickness. *Dev. Cell* **25**, 256-269. doi:10.1016/j.devcel.2013.04.005

**Ule, J., Jensen, K., Mele, A. and Darnell, R. B.** (2005). CLIP: a method for identifying protein-RNA interaction sites in living cells. *Methods* **37**, 376-386. doi:10.1016/j.ymeth.2005.07.018

**Wang, Y., He, L., Du, Y., Zhu, P., Huang, G., Luo, J., Yan, X., Ye, B., Li, C., Xia, P. et al.** (2015). The long noncoding RNA lncTCF7 promotes self-renewal of human liver cancer stem cells through activation of Wnt signaling. *Cell Stem Cell* **16**, 413-425. doi:10.1016/j.stem.2015.03.003

**Wang, A., Wang, J., Liu, Y. and Zhou, Y.** (2017). Mechanisms of long non-coding RNAs in the assembly and plasticity of neural circuitry. *Front. Neural Circuits* **11**, 76. doi:10.3389/fncir.2017.00076

**Xie, Z. F., Ma, X. H., Ji, W. L., Zhou, G. D., Lu, Y. Z., Xiang, Z. H., Wang, Y. X., Zhang, L., Hu, Y. P., Ding, Y.-Q. et al.** (2010). Zbtb20 is essential for the specification of CA1 field identity in the developing hippocampus. *Proc. Natl. Acad. Sci. USA* **107**, 6510-6515. doi:10.1073/pnas.0912315107

**Xu, L. C., Zheng, Y., Li, X. J., Wang, A. D., Huo, D. W., Li, Q. L., Wang, S. K., Luo, Z. Y., Liu, Y., Xu, F. Q. et al.** (2021). Abnormal neocortex arealization and Sotos-like syndrome-associated behavior in Setd2 mutant mice. *Sci. Adv.* **7**, eaba1180. doi:10.1126/sciadv.aba1180

**Yao, B., Christian, K. M., He, C., Jin, P., Ming, G.-L. and Song, H.** (2016). Epigenetic mechanisms in neurogenesis. *Nat. Rev. Neurosci.* **17**, 537-549. doi:10.1038/nrn.2016.70

**Yoon, K.-J., Vissers, C., Ming, G.-L. and Song, H.** (2018). Epigenetics and epitranscriptomics in temporal patterning of cortical neural progenitor competence. *J. Cell Biol.* **217**, 1901-1914. doi:10.1083/jcb.201802117

**Zhao, C., Deng, W. and Gage, F. H.** (2008). Mechanisms and functional implications of adult neurogenesis. *Cell* **132**, 645-660. doi:10.1016/j.cell.2008.01.033